(5) 611 800

408 472

SECOND QUARTERLY REPORT

THIN FILM ACTIVE DEVICES

22 September to 22 December 1962

James P. Spratt

Contract No. DA-49-186-ORD-1056

with

Harry Diamond Laboratories

PHILCO
A SUBSIDIARY OF Ford Motor Company
SCIENTIFIC LABORATORY

$8.10

Copy No.

SECOND QUARTERLY REPORT

THIN FILM ACTIVE DEVICES.

22 Sept[illegible] to 22 Dec[illegible] 1962

James P. Spratt

Contract No. DA-49-186-ORD-1056

with

Harry Diamond Laboratories

J046-2

PHILCO

A SUBSIDIARY OF Ford Motor Company

SCIENTIFIC LABORATORY

BLUE BELL, PENNSYLVANIA

LIST OF ILLUSTRATIONS

LIST OF ILLUSTRATIONS (Cont)

SECTION I

PURPOSE

This is the second quarterly report, covering the period 22 September 1962 to 22 December 1962, on Contract No. DA-49-186-ORD-1056 with Diamond Laboratories for work on thin film devices.

The purpose of this work is to conduct a research and development program directed toward the development of an active thin film triode device dependent upon tunneling for its gain mechanism. This program will be carried out in such a way to allow the early fabrication of thin film triodes, the extension and refinement of thin film techniques related to fabrication, and the extension and refinement of the theoretical understanding of these devices.

SECTION II

ABSTRACT

The use of evaporated, rather than thermally grown, layers of Al_2O_3 has alleviated the shorting problem in the MEA tunnel emission device. High input impedance devices showing transconductance values as high as 25,000 μmhos have been obtained in this way. A tentative equivalent circuit for the device is presented.

Studies of the conduction processes in CdS-Al_2O_3-Al diodes continue. Thin films of CdS show resistivities of approximately 0.1 ohm-cm, mobilities of 10 cm²/V-sec, and carrier concentrations of 7 x 10^{16}/cm³.

SECTION IV

FACTUAL DATA

A. Introduction

Most of the studies of hot electron structures currently underway involve investigations of metal-insulator or metal-semiconductor interfaces for emitters and/or collectors. In the first quarterly report under this contract, several problems associated with such interfaces for these applications were discussed; viz., backscattering out of the collector barrier, injection of a monoenergetic electron beam, etc. There is reason to believe that certain aspects of these problems would be alleviated by using complex interfaces of the metal-insulator-semiconductor type.

Such interfaces have been used sucessfully as high efficiency emitters.[1] In addition, the use of a thin (less than a phonon mean free path) insulator between the metal base film and the semiconductor collector barrier layer should improve the collection efficiency of hot electron triodes. This improvement is based on two phenomena, viz., backscattering and the critical angle for collection as discussed in the First Quarterly Report. To understand this possible improvement, consider a beam of electrons in a metal base film having an energy ΔE in excess of the Fermi energy, and let this beam of electrons be traveling toward a metal-insulator collector barrier of height ϕ_c. Those electrons which pass over this collector barrier then have the possibility of being scattered by phonons in the barrier region. Since phonon scattering results in an isotropic distribution of scattered electrons, some of these carriers will go back into the base film and be lost unless the collector barrier prevents this. A simple metal-insulator barrier will not prevent backscattering into the base since any electron traveling toward the base film will be able to conserve energy and lateral momentum in re-entering the base. If, however, a graded gap collector barrier is used, such as occurs with a metal-insulator-semiconductor barrier, and if the insulator is thin enough so that no phonon collisions occur in this layer, some electrons scattered in the semiconductor will be prevented from re-entering the base due to their inability to conserve lateral momentum at the semiconductor-insulator interface. The necessity for conserving lateral momentum at an interface, discussed in the previous report, results in an effective "cone of collection," i.e., a cone of semi-angle δ within which an electron must strike the barrier in order to cross it. If the barrier is a repulsive one, δ is less than 90° and electrons outside the cone undergo total reflection at the interface. If the barrier is an attractive one, δ is 90° and all electrons can pass. Thus, an M-O-S barrier uses the repulsive barrier existing at the semiconductor-insulator interface to prevent backscattering and thereby improve collection efficiencies.

In addition to high collection efficiency, high output impedance is also a necessary characteristic of a hot electron collector. This is why the semiconductor is needed in the M-O-S collector. High collection efficiency could be assured if one used only a thin insulator backed up by a metal as a barrier, but since base-to-collector tunneling could then occur, the output impedance would be low. In the M-O-S collector, a portion of the base-to-collector voltage drops across the semiconductor, decreasing the output capacitance and increasing the output resistance. Thus, power gain does not suffer.

A theoretical treatment of the problem of collection at M-O-S barriers is underway and will be presented when completed. Meanwhile, an experiment is being developed by Dr. A. Berman of the Philco Scientific Laboratory which will allow direct determination of collection efficiencies in this and other systems. M-O-S diodes are being studied to determine current flow mechanisms, field distributions, etc. Structures are being fabricated with aluminum, aluminum oxide-cadmium sulfide, and the resistivity of the CdS is being varied by heat treatment processes. By varying the resistivity of the CdS, the height of the barrier at the insulator-semiconductor interface can be varied and the output impedance changed. Thus, heat treatment studies can provide interesting clues to the behavior of M-O-S structures as hot electron collectors.

B. Method of Study

Previous data[2] showed tunnel-like I-V characteristics of M-O-S diodes fabricated on germanium substrates. However, very little data was obtained on the evaporated CdS used in these diodes. Therefore, resistivity, mobility, C-V, and J-V data have been obtained on new diodes. The fabrication techniques and characteristics obtained in these experiments are described in the following paragraphs.

1. Fabrication

I-V studies on CdS-Al_2O_3-Al sandwich structures were continued. M-O-S diodes were fabricated on glass substrates so the current flow mechanism of this structure could be studied (see Figure 1). Coevaporated underlays of Cr-Au ~500 Å thick were evaporated on glass substrates. Aluminum films ~2000 Å were deposited at an evaporation rate of 1000 Å/ sec overlapping the Cr-Au underlays. The source-to-substrate distance during the aluminum evaporation was 2 inches. The pressure during the evaporation was 1×10^{-5} mm Hg. The freshly evaporated aluminum film was oxidized for 2 hours at atmospheric pressure in the Bell jar by admitting dry air. The moisture content measured with a Meco water analyzer was 10 p.p.m.

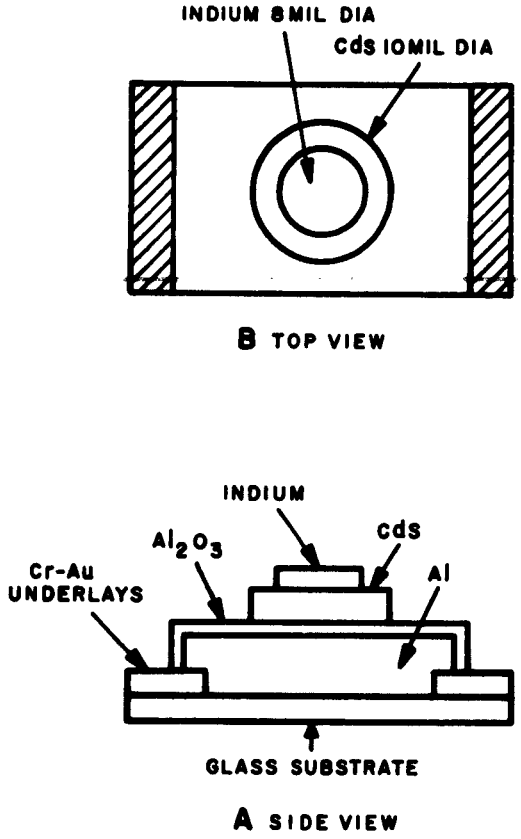

Figure 1 Schematic View of CdS-Al_2O_3-Al Diodes

Next, a 1-micron thick film of CdS, 10 mils in diameter, was evaporated on the Al_2O_3 at a deposition rate of one micron per hour. The evaporant charge is one gram of 'phosphor grade' cadmium sulfide (G.E. No. 113-3-291). This material is evaporated from a formed molybdenium boat at an input power of approximately 45 watts, supplied by a standard high current power supply. To provide a rough check on input power, the voltage drop across the boat was monitored during deposition, and found to be typically about 0.5 volts. Because of the long time required to complete such a deposition, some heating of the system by the boat does occur. To minimize this, water cooled feed-throughs are used. In spite of this, the bell jar is hot to the touch at the completion of a run, and the temperature of an uncooled substrate could rise as much as 100°C by the completion of deposition.

To prevent spattering of the evaporant charge during evaporation, the CdS is pelletized into fragments between 1/16'' and 1/8'' mesh size. These fragments are then loaded into the cone-shaped boat and evaporated in a conventional Kinney PW 400 oil-pumped vacuum system. Prior to deposition, a brief (5-minute) outgassing is conducted, followed by deposition onto a substrate six inches from the source. Deposition rate is monitored by observing interference in a sample film. The monitor used consists of a six volt switchboard lamp, a filter, and a CdSe photoconductor. The combination of filter and photoconductor peaks at 0.73 microns. The output of the CdSe detector thus is an interference function, giving the thickness of the deposited film as a function of time. The relationship governing the film thickness versus time is

$$d(t) = [2k(t) + 1] \frac{\lambda}{4n\cos\phi'}$$

where d(t) is the film thickness,
k(t) is the order number, which increases as d increases,
λ is the wavelength (0.73μ),
n is the index of refraction of the film, and
ϕ' is the angle of refraction in the film.

An indium counter-electrode, eight mils in diameter, is then evaporated on the CdS to provide ohmic contact. Silver paste is used to contact both the indium and the Cr-Au underlays.

Two types of M-O-S diodes were fabricated according to the above described procedure. In one type the CdS was evaporated on the Al_2O_3 grown in dry air at atmospheric pressure for two hours. In the second type of diode the Al_2O_3 was grown under the same conditions, but prior to evaporating the CdS, the substrate was heated to 200°C in vacuum of

1×10^{-5} mm Hg. During the CdS evaporation the substrate temperature was maintained at 200°C. Heating the substrate during deposition in this manner is known to increase the resistivity of evaporated CdS films. In the first diode the temperature of the aluminum film did not exceed 30°C during the entire CdS evaporation. Thus, in accordance with the plans for this quarter, the effect of CdS resistivity on diode properties could be evaluated. The I-V characteristics of these diodes were measured with a Tektronix transistor curve tracer #575.

In this measurement, a half sine wave of maximum voltage V_M and 60 cps frequency is applied to the diode. This voltage also drives the x-axis of an oscilloscope. Another voltage, proportional to the current passed by the diodes, drives the y-axis. Thus, an I-V characteristic of the device is obtained for voltages from 0 to V_M. It has been found that the current drawn at a voltage $V \leq V_M$ depends on the magnitude of V_M, i.e., that these diodes remember the voltage which has previously been applied to them. Figure 2 shows an example of this effect, curve 1 being the characteristic obtained for V_M=1.8 volts, while curve 2 is the characteristic obtained for V_M=2.3 volts. The slope of the ln J versus V characteristic is the same, but the magnitude of the current is different. Similar effects have been seen in many metal-oxide-metal structures, and are felt to be due to the Al_2O_3 layer. Studies are underway to determine the cause of this drifting.

To obtain I-V data when "drifting" of this type is present, it is necessary to use a somewhat different technique from that normally employed. First, the magnitude of the V_M is set at the level desired. Then the y-axis sensitivity of the scope is increased by the factor desired (e.g., 100x) so that only a fraction of the entire I-V characteristic is seen on the scope. (In doing this one must be sure that the origin of the trace does not shift even slightly, or the resultant data will not match the rest of the curve.) This portion of the overall characteristic can then be obtained and matched with that obtained with the y-axis sensitivity at 10x or 1000x. In this way a complete I-V characteristic for a given V_M can be obtained.

The diodes studied to data show similar J-V characteristics in both forward (Al biased +) and reverse (Al biased-) directions. Figure 2a is representative of the functional dependence seen. This is similar, in both magnitude and slope, to that obtained for metal-oxide-metal diodes of the same oxide thickness (see Figure 3) and indicates that the full applied voltage drops across the oxide.

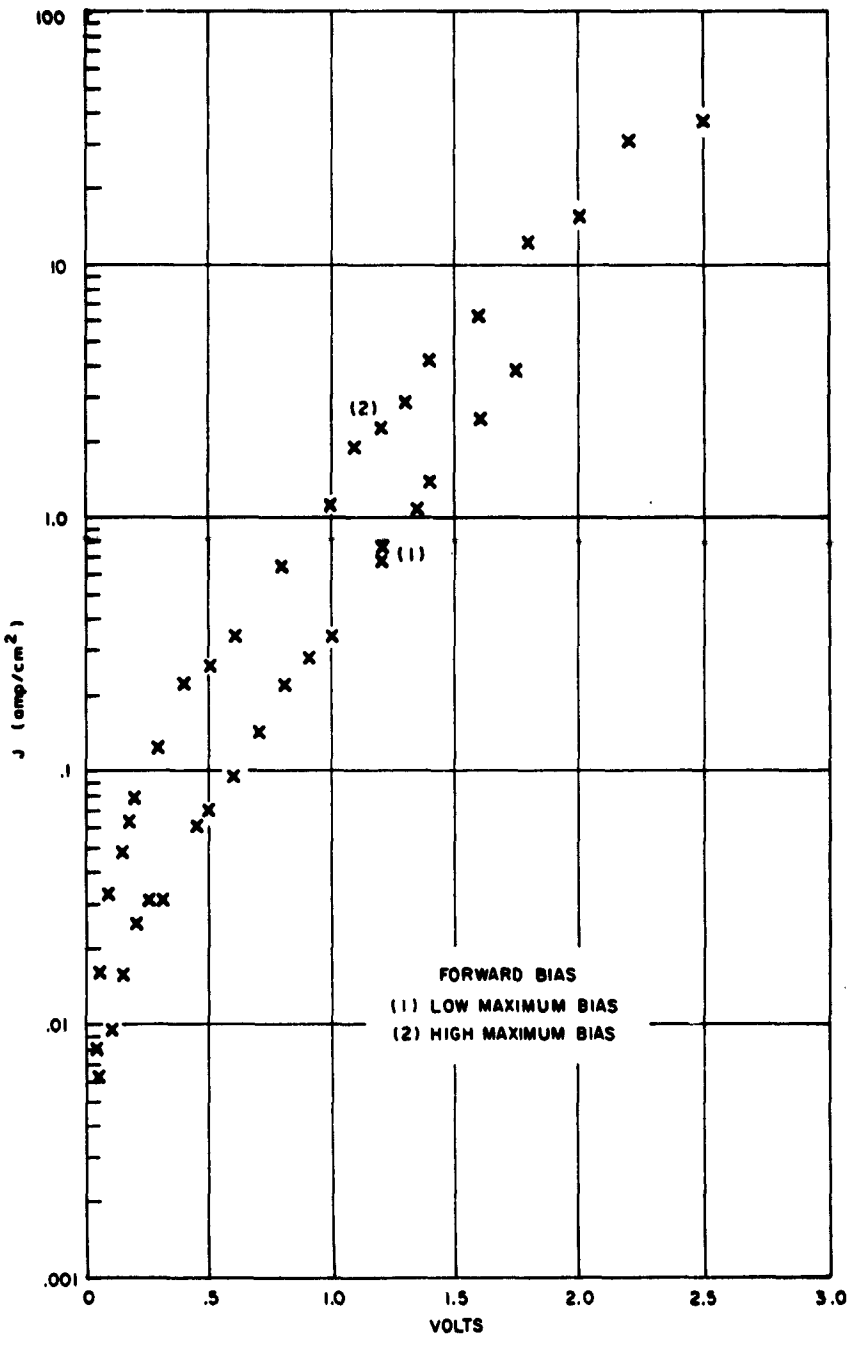

Figure 2a CdS-Al_2O_3-Al Diode Annealed (Forward Bias)

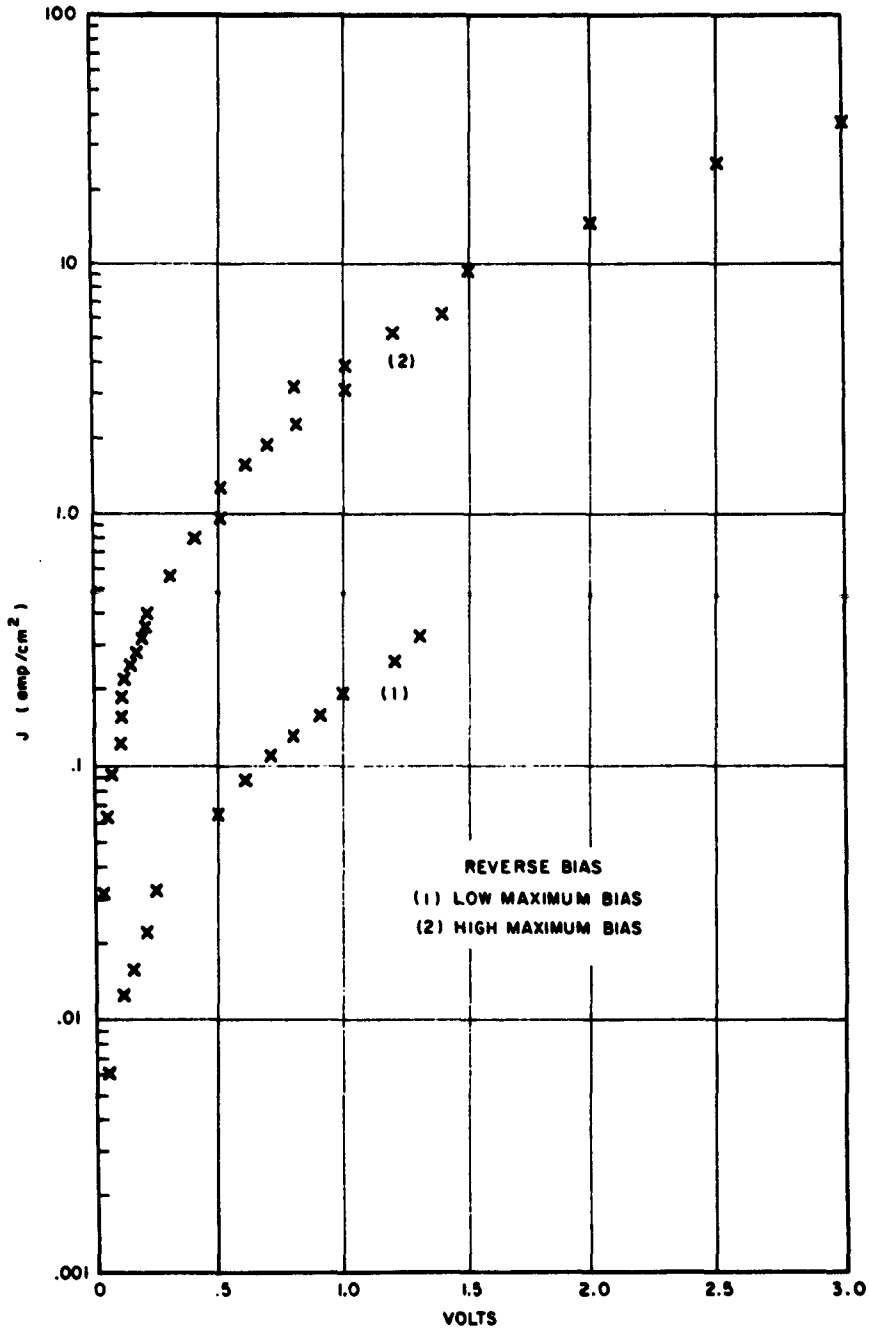

Figure 2b CdS-Al_2O_3-Al Diode Annealed (Reverse Bias)

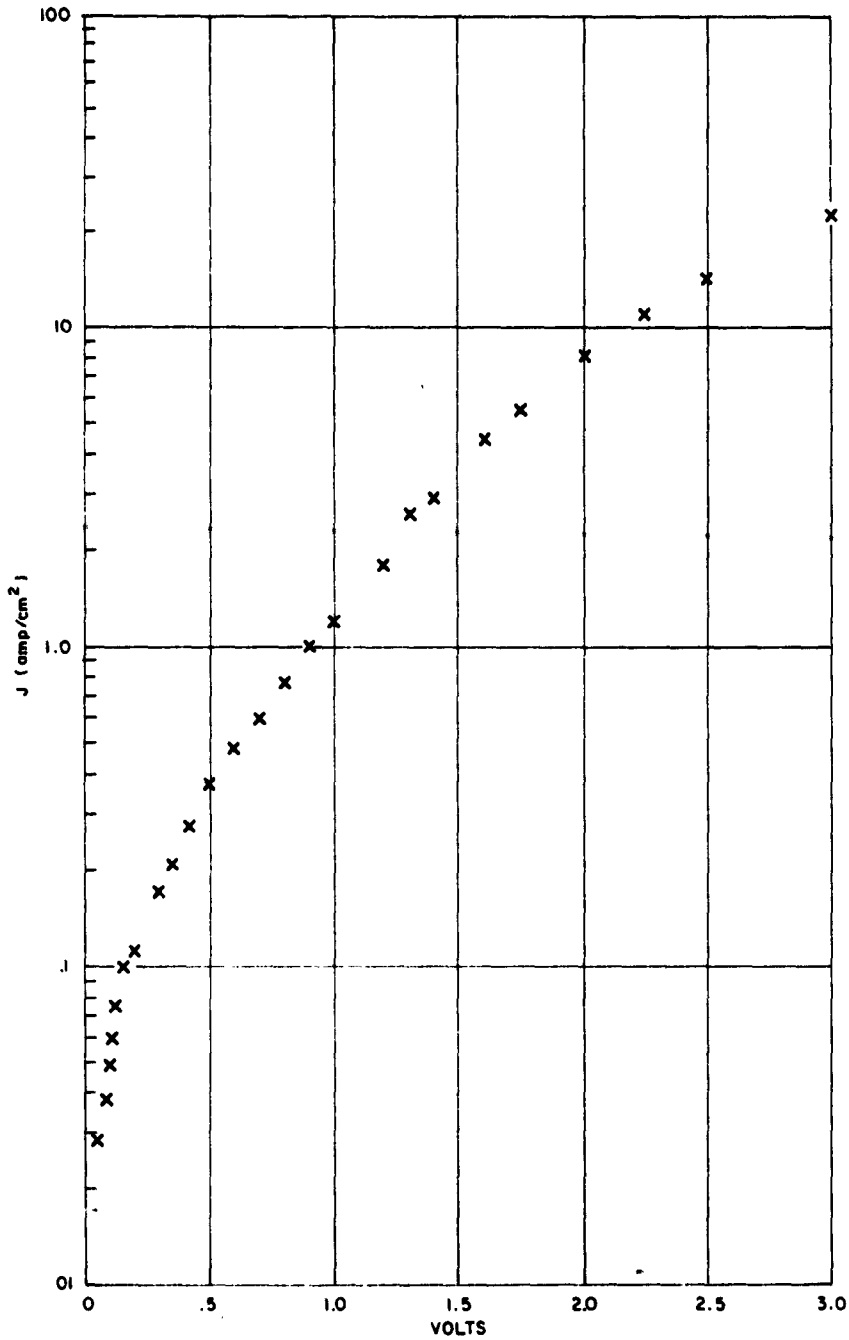

Figure 3 Current Density-Voltage Characteristics for Slide No. 3

2. Capacitance Voltage Characteristics

Small signal (~1 mv) capacitance of CdS-Al_2O_3-Al structures fabricated on glass substrates has been measured at 600 kc on a type 601 Wayne-Kerr impedance bridge. Typical results for diodes which were not heated prior to this Cd evaporation are presented in Figure 4. The effective barrier thickness d/k_1 for these diodes is shown to be 2 Å at zero bias voltages of 1.5 volts.

$$\frac{d}{k_1} = \frac{\epsilon_0 A}{C}$$

where ϵ_0 = permittivity of free space, A = electrode area, and C = measured capacitance. This effective thickness varies by + 70 percent for reverse bias voltages of 1.75 volts, and -20 percent for forward bias voltages of 1.5 volts.

The diodes which were heated to 200°C prior to the CdS evaporation had an effective barrier thickness $d/k_1 \sim 15$ angstroms at zero bias. Typical results are presented in Figure 5. This increase in effective barrier thickness for heated diodes could not be entirely attributed to the increase in Al_2O_3 thickness during heating. The oxide of aluminum grown in dry air at atmospheric pressure thickens at a rate of ~ 10 Å/100°C.[3] Since the above mentioned diodes were heated to 200°C at pressures $<1 \times 10^{-5}$ mm Hg, one would expect that the aluminum oxide thickness would not increase by more than a factor of two. This could not account for the increase in effective barrier thickness for heated CdS-O-M diodes. These results are, however, indicative of the effect of substrate temperature on CdS resistivity.

3. CdS

Hall measurements were made on unannealed CdS films evaporated under identical conditions as in the diodes discussed above. The elimination of the effect of associated thermomagnetic and galvanomagnetic current (Righi-Leduc and ohmic) effects is achieved by taking a series of four measurements.[4] These measurements are taken by reversing the magnetic field and sample current in all possible combinations. From the Hall voltage given by V_H where

$V_H = RJH/b$;

J = the current density,

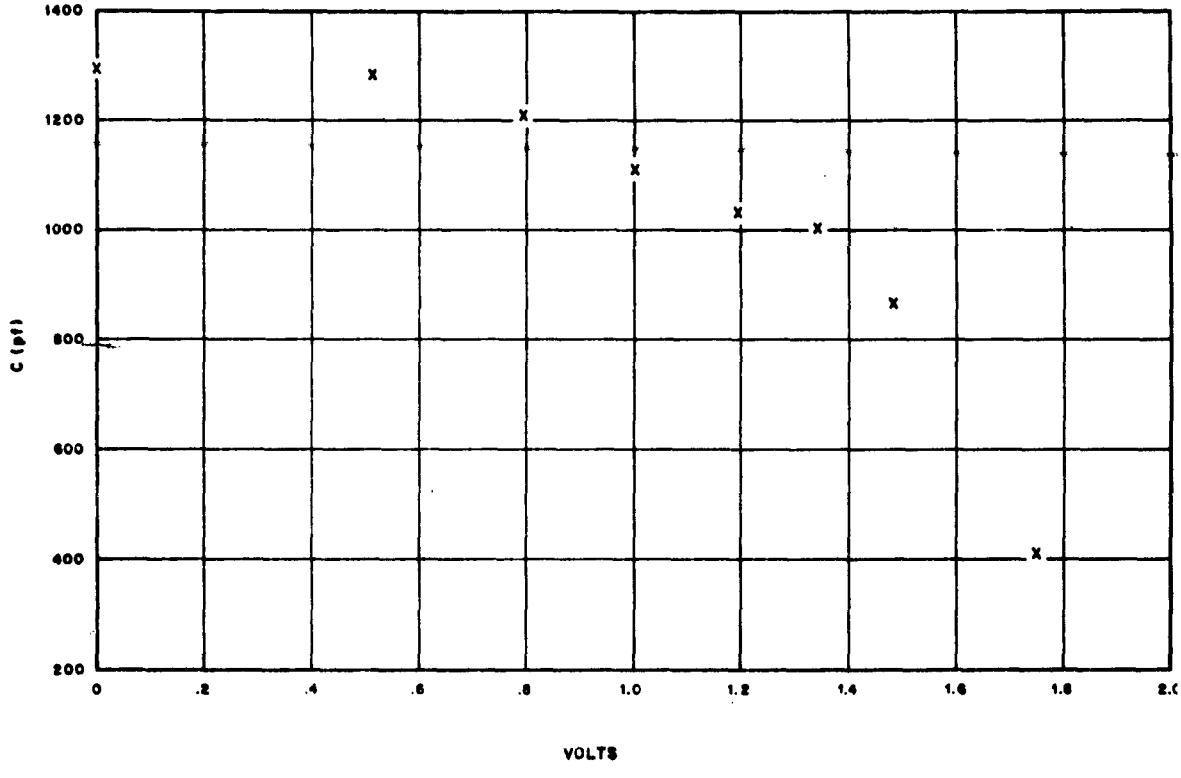

Figure 4a Capacitance vs. Voltage for CdS-Al_2O_3-Al Diode, Unannealed (Al Biased Negatively)

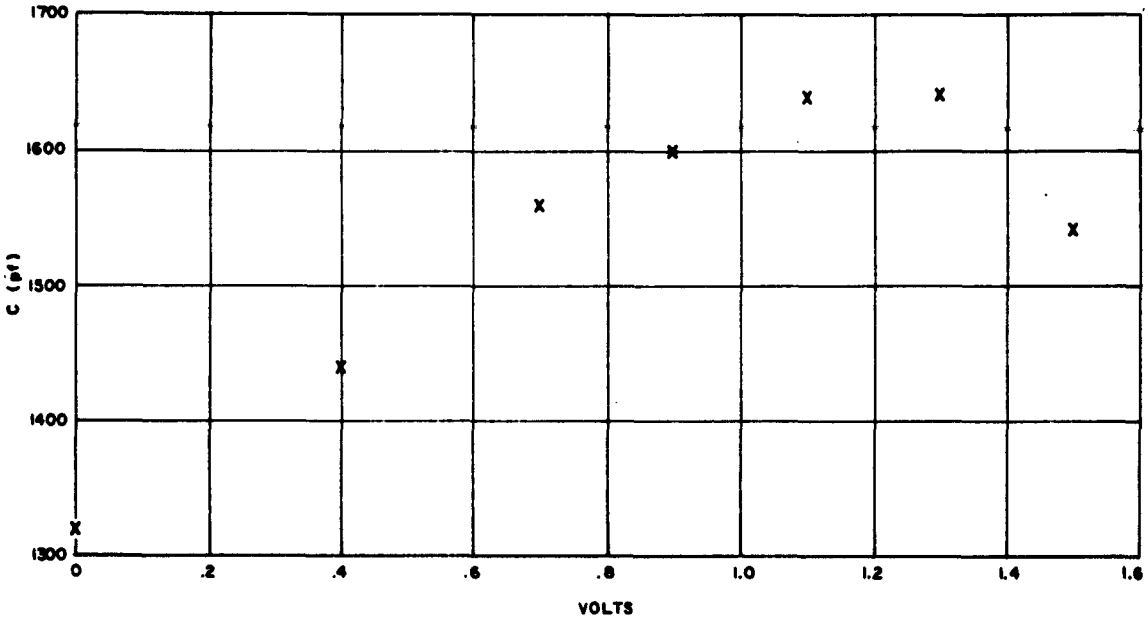

Figure 4b Capacitance vs. Voltage for CdS-Al_2O_3-Al Diode, Unannealed (Al Biased Positively)

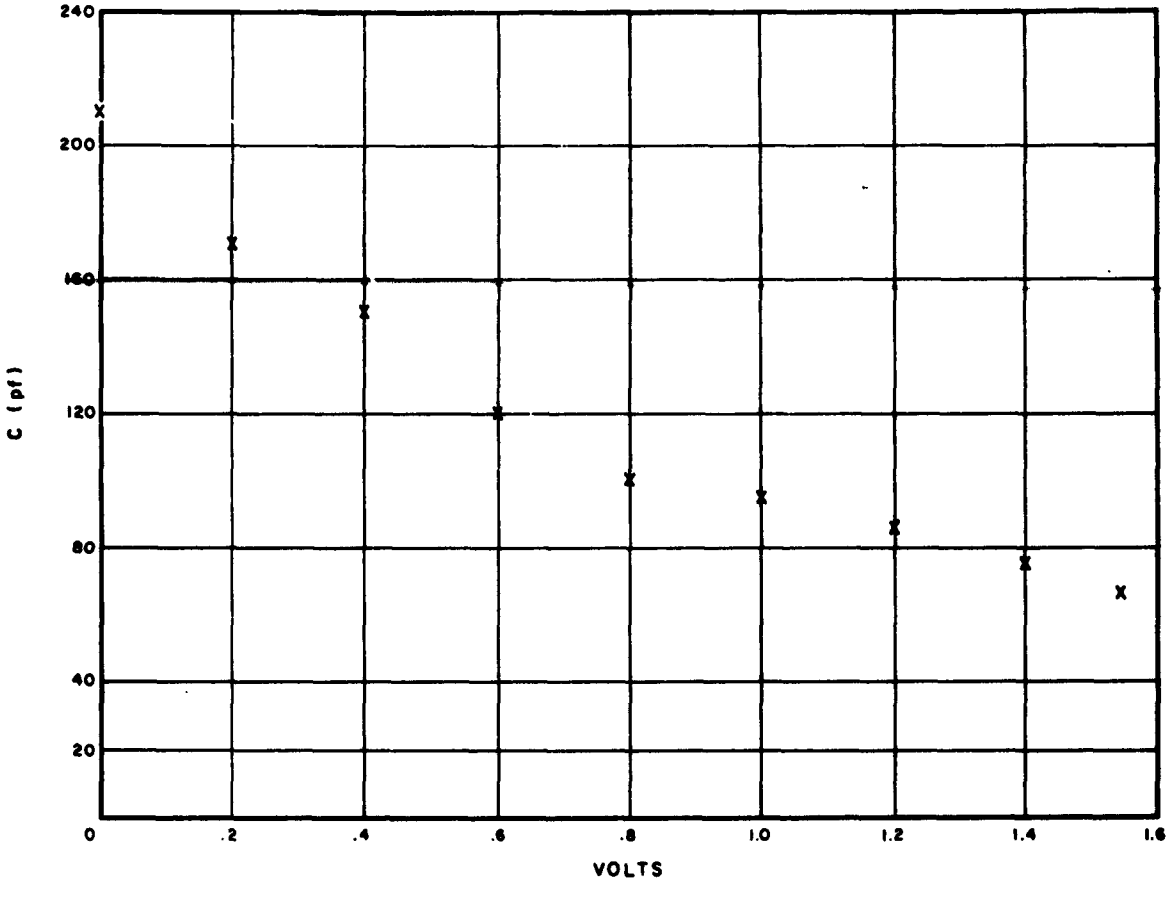

Figure 5a Capacitance vs. Voltage for CdS-Al_2O_3-Al Diode, Annealed (Al Biased Negatively)

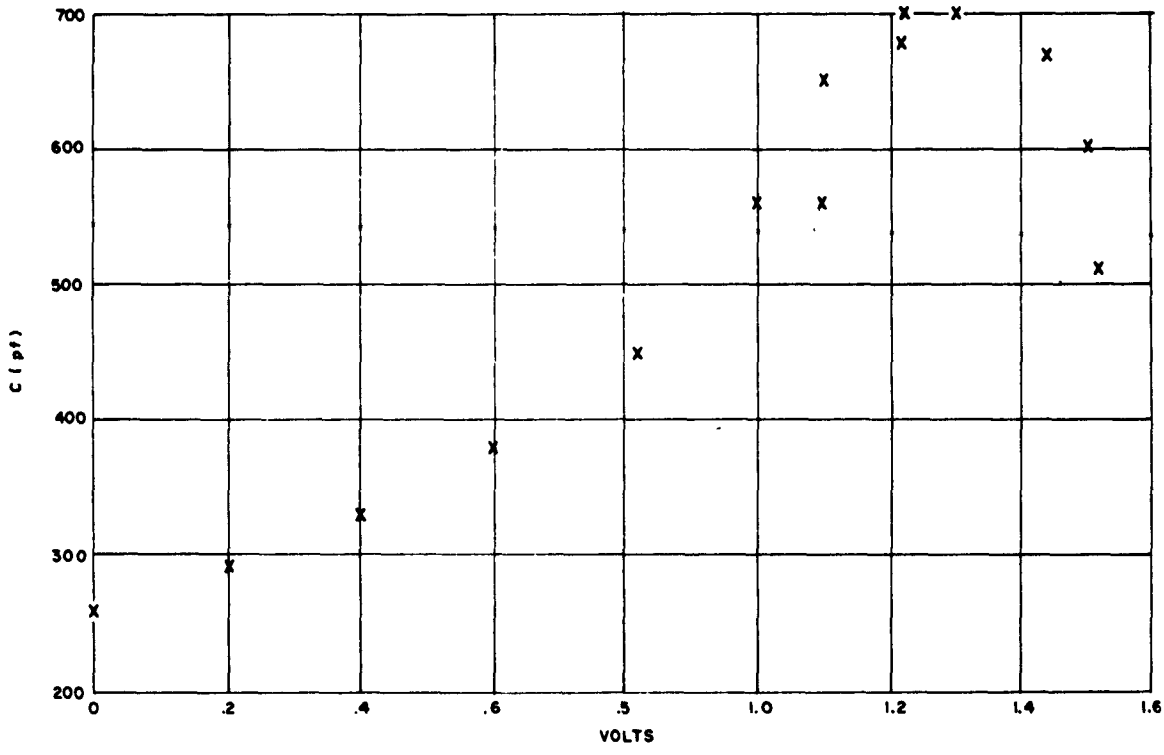

Figure 5b Capacitance vs. Voltage for CdS-Al_2O_3-Al Diode, Annealed (Al Biased Positively)

H = the applied magnetic field,

b = the sample thickness, and

R = the Hall constant,

one can calculate the Hall constant R. The carrier concentration, n, and mobility, μ, can then be determined if the resistivity is known, since

$$R = 3\pi/8nec \approx \mu\rho/c.$$

The Hall voltage on unannealed CdS films was $V_H = 0.01$ mv. The calculated Hall coefficient was R = 1. Placing these values into the above expressions and relating Hall coefficient, carrier concentration and mobility, one obtains a value of $n = 7 \times 10^{18}$ carriers per cc, and mobility $\mu = 10$ cm^2/volt sec. The measured resistivity for these films is $\rho = 0.087$ ohm-cm.

C. The MEA Device

As reviewed in the last quarterly report a serious fabrication problem had been encountered with this device, viz., the tendency of the emitter and base films to short. The thermal oxidation of aluminum was found to be an unsatisfactory method of producing the insulating region of the MEA structure. A method of preparation of the oxide dielectric by the evaporation of aluminum in an oxygen atmosphere was developed. The results of this study are discussed below, and preliminary evaluations of the devices produced by this method are shown.

1. Evaporated Aluminum Oxide Films

Attempts to prepare metal oxide coatings by evaporating metals in pressures of oxygen in the 0.1 to 10 micron range have been reported.[5,6] This method was used to study the properties of insulator films produced by the evaporation of aluminum in a partial pressure of oxygen in the range of 10^{-3} mm Hg.

Initially the procedure used in the Philco laboratory was to evaporate a film of aluminum or gold onto a glass substrate using a contact mask to produce a metallic area of 0.125 inch x 0.50 inch. This was done in an oil diffusion system at a pressure of 5×10^{-6} Torr. The glass substrate was removed from the system to permit a second mask to be inserted which would overlap the metallic area by 0.025 inch on the long edge and on the ends by 0.010 inch. The system was pumped down to a

pressure of 5×10^{-5} Torr and backfilled with oxygen to 1×10^{-3} Torr. This pressure was controlled by bleeding oxygen into the system through an Edwards high vacuum needle valve, and was measured with a Consolidated Vacuum Corporation cold cathode discharge gauge mounted in the base plate. It was necessary to maintain a very slow evaporation rate of the aluminum. If the evaporation rate was too rapid, a decrease in pressure was observed, and the resulting films had a metallic appearance and a low resistance. As the evaporation rate was decreased, the oxygen pressure increased, and the resulting films were transparent. The optimum conditions of pressure and evaporation rate were difficult to maintain because the charge tended to oxidize on the surface, causing formation of a cocoon of oxide around the molten metal.

As the final step a metallic film was evaporated onto the oxide overlapping the edge of the first metallic electrode. Figure 6 shows a cross-sectional view of this diode. Figure 7 shows the curve tracer characteristics of a metal-oxide-metal sandwich on glass. These characteristics are typical of those observed when the aluminum oxide evaporation is optimized, and the impedance is greater than 0.5 megohms up to 6 volts. The breakdown voltage was 9 volts.

Germanium-aluminum oxide-aluminum diodes were fabricated during the second phase of the development of this process. Capacitance as a function of voltage typical of this structure is shown in Figure 8. Two distinct regions are apparent in the capacitance versus voltage characteristics of the diode. In the first region the capacitance is constant while in the second region capacitance decreased with voltage as $V^{-1/2}$. This first region represents the large capacitance caused by the oxide layer, and will be determined solely by geometry.

As the applied voltage is increased, this capacitance remains constant until the germanium surface charge is depleted. In this case, the capacitance remains constant until the applied voltage is increased to about 1 volt. This will vary depending upon the oxide thickness and the surface state density. The decrease in capacitance of the M-O-S diode with further increase in voltage is similar to that of a surface barrier diode. It is caused by widening of the depletion layer in the germanium, brought about by the need of additional charge to satisfy the applied voltage.

2. Triode Fabrication

Triode structures were fabricated as a third phase of the program. In this case the chemically polished n-type germanium was

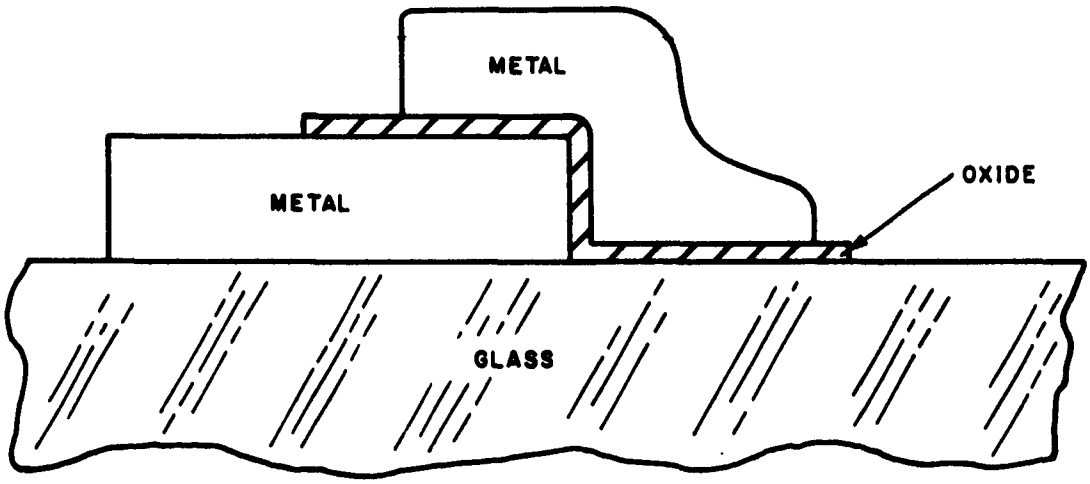

Figure 6 Cross-Sectional View of Evaporated Oxide Device

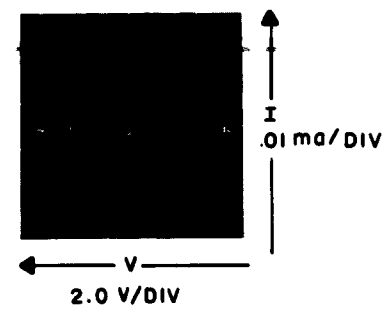

Figure 7 Typical I-V Charachertistics of Al-Evaporated Al_2O_3-Al Sandwich on Glass

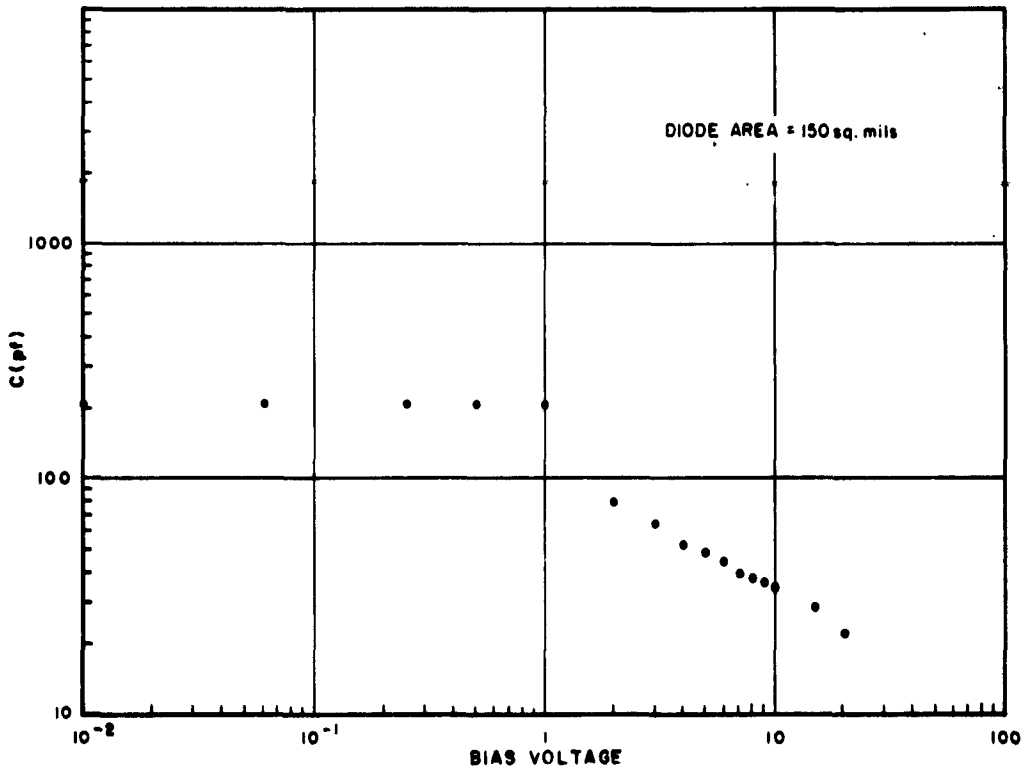

Figure 8 C vs. V at 5 Megacycles for Ge-Al_2O_3-Al Diodes (Al Biased Negatively)

mounted onto TO18 headers using Au-0.5 percent P solder. A mask yielding a metallic strip 0.015 inch x 0.010 inch was used for the emitter evaporation. A tungsten filament containing 0.5 gm of high purity aluminum charge was placed directly above the substrate with a source-to-substrate distance of 17cm. Metal electrodes, 300 Å thick, were deposited at a rate of 1000 Å per second at a base pressure of 6×10^{-5} Torr. The specimens were removed from the system to change masks for the oxide deposition. The source-to-substrate distance was maintained at 17 cm during the oxide evaporation, but the Al charge was reduced to 0.1 g. The oxygen pressure was maintained at 1×10^{-3} Torr while the filament temperature was increased (from room temperature to 900°C in 250 seconds). By this procedure the oxide was deposited upon the substrate for 45 seconds. It is estimated that the evaporation rate is on the order of 1 Å per second for a thickness of approximately 45 Å. At this time no attempt has been made to vary the oxide thickness.

Measurements of the thickness of the oxide films by the Tolansky method have not succeeded. A large difference in the sticking coefficient of silver on glass and Al_2O_3 has been observed. (This was discovered by evaporating a thin Ag layer on a glass slide half of which was covered with Al_2O_3. It was noted that the Ag film in direct contact with the glass was opaque, while that in contact with the Al_2O_3 was still translucent. Thus the sticking coefficient of Ag on glass is much higher than on Al_2O_3.) This introduces an error in the measurement of oxide films less than several hundred angstroms thick. A modulating electrode of aluminum was subsequently deposited using the procedure as used for the emitter deposition. Contact was made to the metallic areas with silver paste after which the devices were encapsulated in a dry nitrogen atmosphere.

A cross-sectional view of the device is shown in Figure 9. The term modulator has been applied to the second metal electrode deposited. This term best describes the function of this electrode.

More than 80 percent of the triodes were active when the desired conditions of pressure and evaporation rate were maintained during the aluminum oxide evaporation. This indicates that the shorting problems encountered previously can be eliminated by using evaporated rather than thermally grown layers of Al_2O_3.

3. Triode Evaluation

Figures 10A and B show typical common modulator output and transfer curves for an evaporated oxide device having an electrode 15 mils long.

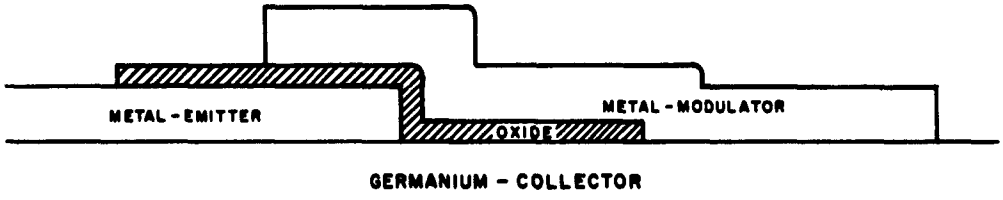

Figure 9 Cross-Sectional View of MEA Device Using Evaporated Al_2O_3 Layer

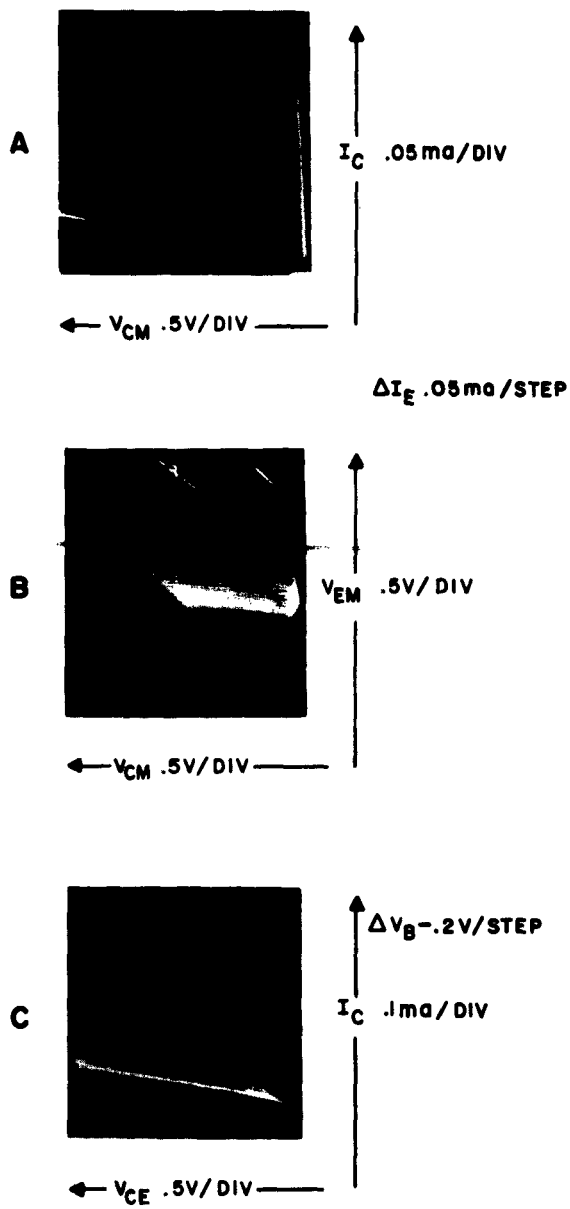

Figure 10 Output Characteristics of MEA Device Using Evaporated Al_2O_3 Layer

The first film to be deposited is used as the emitter of the device and biased negatively with respect to the second film which serves as the modulator. An α of approximately unity and a high input impedance are observed. In the reverse mode, that is when the second film is biased negatively with respect to the first film, vastly dissimilar output curves are observed, i.e., $\alpha < 0.02$. This can be explained in terms of the nonsymmetrical geometry of the device (see Figure 9). In the normal mode the current gain is due to controlled field emission, and in the reverse mode it is probably caused by some other mechanism, possibly surface-state modulation.

This same unit in the grounded emitter configuration shows a nonsaturating β when driven with constant current steps. An active transconductance (Figure 10C) was exhibited by the unit when driven from a constant voltage source.

The low-frequency small-signal equivalent circuit shown in Figure 11 has been deduced from the data available. This equivalent circuit includes the parasitic feedback resistance, R_{cm}, caused by overlapping of the modulator electrode onto the germanium collector surface. Mask revisions are underway to eliminate this. Conduction through the oxide may be responsible for some remaining feedback. This will be investigated with the new geometry.

Measurements have been made of both the common modulator and common emitter characteristics of some devices as a function of temperature. Figure 12 shows I_C versus I_E in the grounded modulator configuration from 20° C to -100°C. The slope, α, proved to be independent of temperature. It is seen that for $I_E = 0$, I_C does not vanish. This is due to the leakage current flowing between the modulator and the collector. When the direct contact between modulator and collector is eliminated, this leakage component will be largely eliminated.

Figure 13 shows the emitter impedance grounded modulator versus temperature. It is seen that there is a general tendency for the emitter impedance to rise with decreasing temperature, the data obtained at -50°C being the exception. (It is probable that the -50°C data is in error for some reason, since similar data taken after the end of the second quarter show smooth increases of impedance with decreasing temperature.) Figure 13 presents data useful in the analysis of the gain mechanism of MEA triodes. It does not give the input impedance of the device, since in operation these devices are run with the emitter grounded. (By analogy, this data is similar to the cathode current-voltage characteristic of a

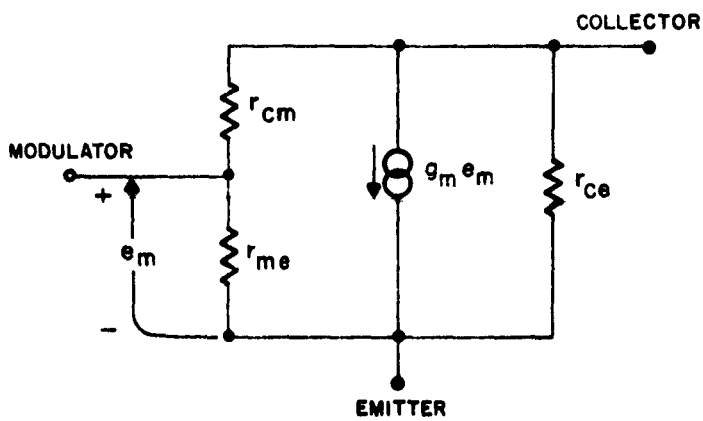

r_{ce} - The Collector - Emitter diode reverse resistance.

r_{me} - The Modulator - Emitter resistance due to both ohmic conduction and tunneling through the oxide.

r_{cm} - The Collector - modulator resistance due chiefly to the overlap of the modulator film onto the collector. (this will be practically eliminated by geometry changes).

Figure 11 Proposed MEA Low-Frequency Equivalent Circuit

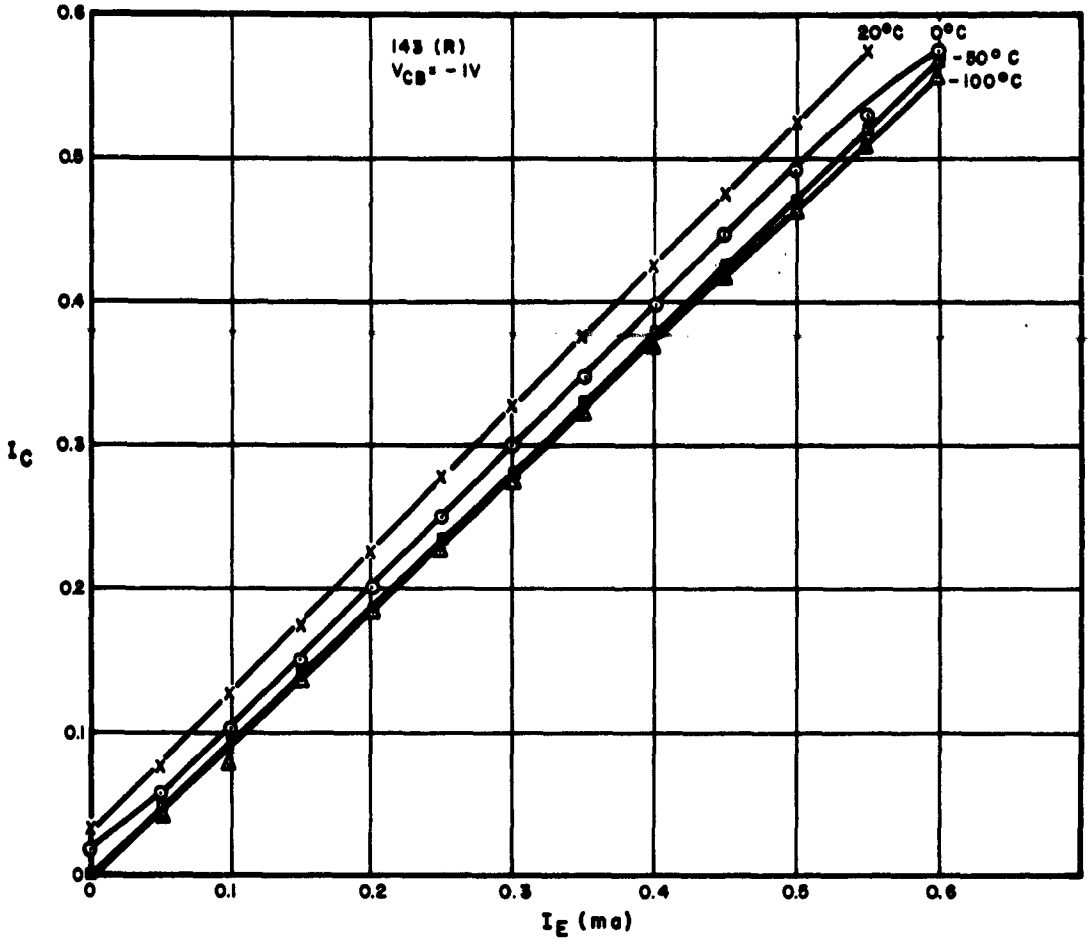

Figure 12 I_C vs. I_E for MEA Device as a Function of Temperature

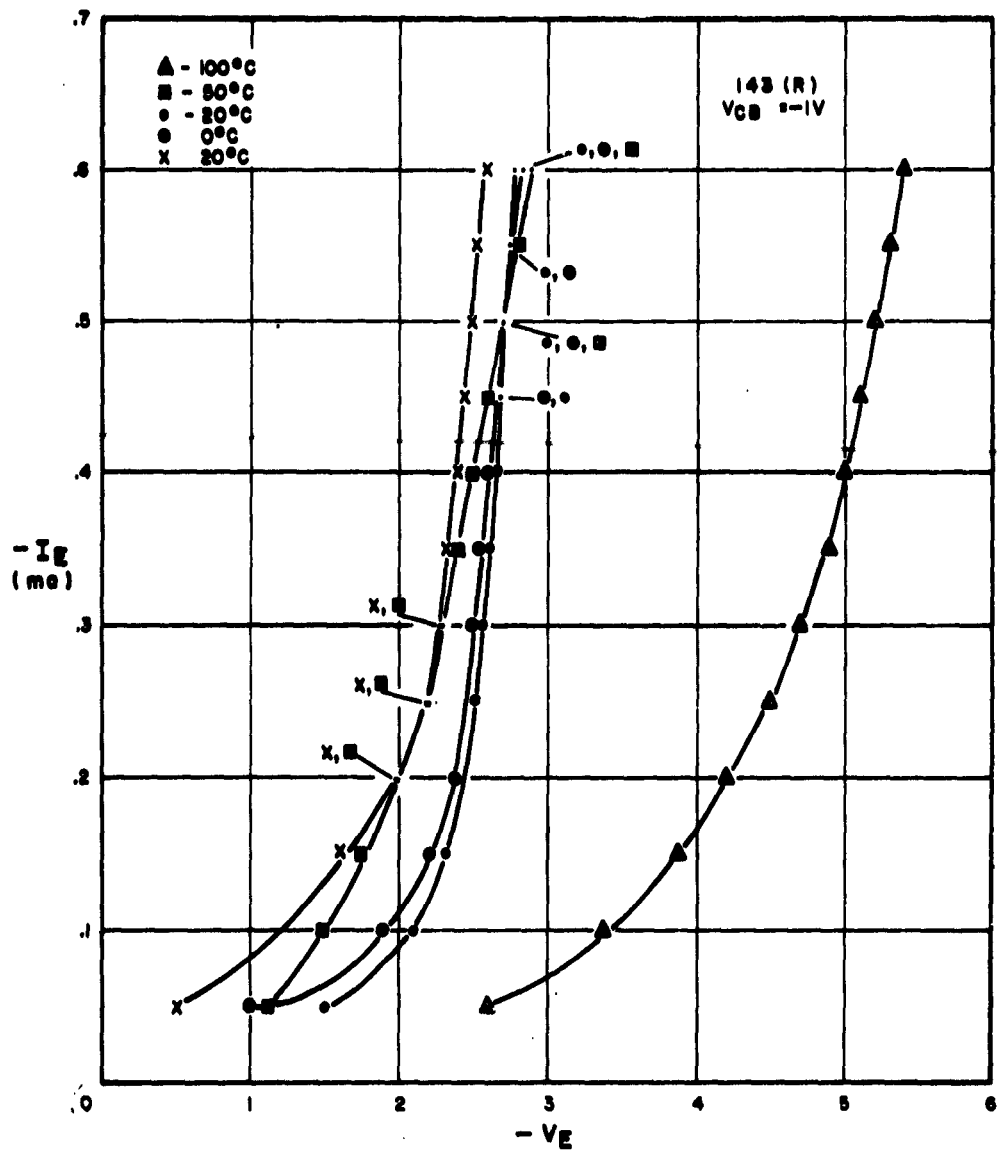

Figure 13 Input Curves for MEA Device vs. Temperature

triode obtained with the grid grounded.) Thus, the fact that the impedances shown in Figure 13 are low does not contradict the statement that these devices have high input impedance.

The collector current for various emitter-modulator voltages versus temperature is shown in Figure 14. The slope is the transconductance, g_m. From preliminary data g_m appears to be relatively constant to -50°C. For these devices the saturation resistance is approximately equal to $1/g_m$. If g_m is temperature dependent, the saturation resistance will also vary. Additional studies are necessary to determine the equivalent circuit elements and their temperature dependence.

Figure 15 shows common modulator output (a) and transfer (b) curves for a unit having a 125 mil line length. Figure 15c presents common emitter output data for the same unit, showing a transconductance g_m of greater than 20,000 micromhos. This high g_m may in part be due to the rather long line length (ℓ) used (g_m should increase linearly with increasing line length). Further studies are necessary to show the dependence of g_m on ℓ and other parameters.

The foregoing has shown the feasibility of using evaporated insulators to achieve isolation between the emitter and the electrode controlling emission (called the modulator). In the structures described here however, the modulator electrode is wider than necessary and actually overlaps onto the body of the collector. New masks are being built which will allow the modulator to be located entirely on the evaporated insulator, thereby eliminating a parasitic resistance element..

4. Equipment

A mask changer for use in the Ultek Hi Vacuum system has been designed, and construction is nearly completed. This will permit the complete fabrication of devices using the evaporated Al_2O_3 insulator without removing the substrate from the system.

The stringent requirements for control of both source temperature and oxygen pressure during Al_2O_3 evaporation led to the design of a control system for this purpose. Preliminary tests have been made with a breadboard. This work will be continued.

Several methods for monitoring the evaporation rate are currently being studied.

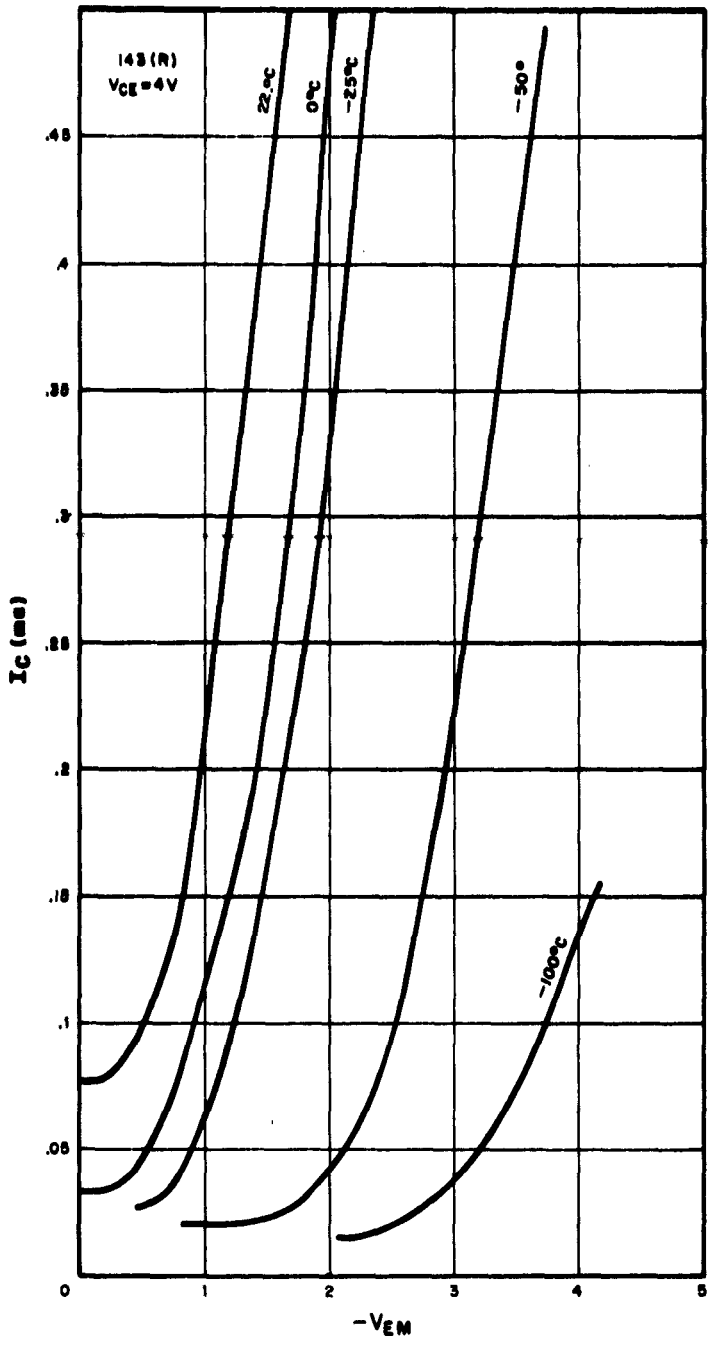

Figure 14 Transfer Curves of MEA Device vs. Temperature

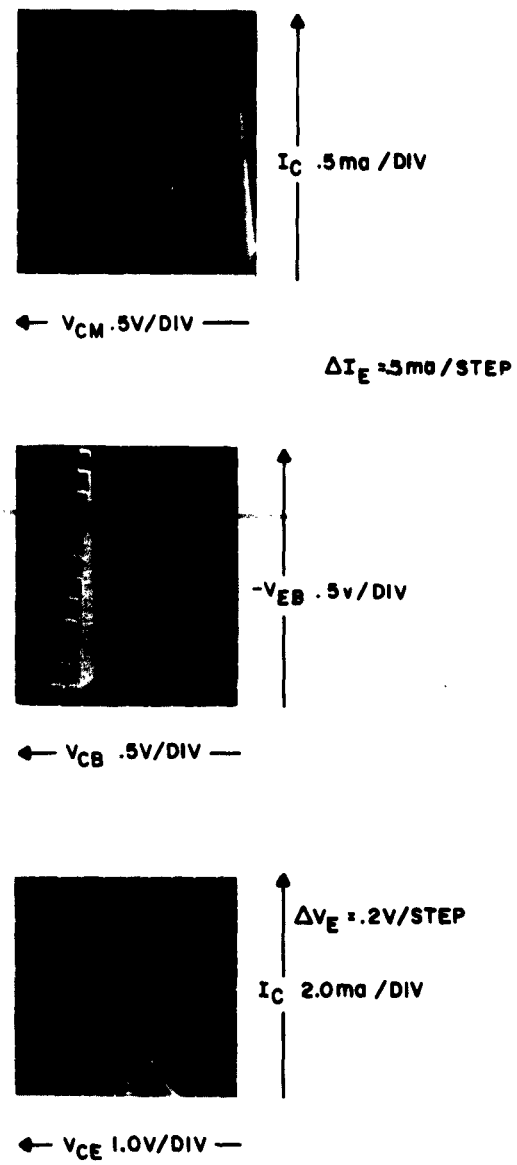

Figure 15 Output and Transfer Curves for High Gain MEA

SECTION V

CONCLUSIONS

High input impedance triodes showing very high values of transconductance can be produced by means of the MEA structure when evaporated insulating films are used between emitter and modulator.

As expected, a profound effect on the electrical characteristics of CdS-Al_2O_3-Al diodes was produced by heat treating the CdS. Unannealed films of CdS produce diodes quite similar to metal-oxide metal diodes, while heat treating increases diode impedance and decreases capacitance.

SECTION VI

PLANS FOR NEXT QUARTER

Evaluation of the present MEA triode structure will be continued. Mainly static characteristics have been analyzed to date. Additional a-c measurements will be made.

The effect of geometry, particularly oxide thickness, on the performance of the MEA structure will be evaluated. The masks used in the evaporation of the modulator electrode have been redesigned to allow the metal to be deposited entirely on the oxide layer, thereby eliminating the parasitic impedance, r_{cm}, discussed in the prior section. This mask will be available soon.

A method for accurately determining the thickness of the insulator still must be developed.

Continued studies will be made of the CdS-Al_2O_3-Al diode structure to determine whether the current flow through the oxide layer is due to tunnelling or carrier transport through the conduction band of the oxide.

An experiment is being designed to determine experimentally the transport and collection efficiencies of a directed, monoenergetic hot electron beam in a metal. In this experiment, the metal base film to be studied is deposited on the desired collector barrier material and contacts made to both these regions. The work function of the base is then lowered to some predetermined value by depositing on its surface a monolayer (or fraction thereof) of barium oxide. At this stage, a low energy electron beam, obtained by means of an external gun, impinges on the metal base film, and the fraction of the beam current, fc, passing through the base film and out the collector is measured. By determining the variation of fc with the base film thickness and the energy of the electron beam, the transport and collection efficiencies can be determined.

SECTION VII

REFERENCES

1. Spratt and Witt, A Metal Interface Amplifier Device, Solid-State Device Research Conference, University of New Hamsphire, July 1962. (included as Appendix A)

2. Ibid.

3. Hunter and Fowle, J. Electrochem. Soc., Vol 103, p 482, Sept. 1956.

4. Lindberg, Proc. IRE, Vol 40, p 1414, Nov. 1952.

5. Reichelt, W., U. S. Patent No. 2,964,452, 1959.

6. DaSilva and White, J. Electrochem. Soc., Vol 109, No. 1, 1962.

APPENDIX A

A METAL INTERFACE AMPLIFIER DEVICE

J. P. Spratt and W. Witt

I. INTRODUCTION

A Metal Interface Amplifier is an active solid state triode structure where the gain mechanism utilizes an interface between a metal and an insulator or a semiconductor. Such structures have been under study in an investigation of "hot" electron effects in metal films and the feasibility of using such hot electron effects in devices. At the Device Conference in June 1961, a structure consisting of a gold-aluminum oxide-aluminum sandwich on a germanium single crystal was described.[1,2] This structure exhibited active behavior explainable by "hot" electron injection into, transport through, and collection from the thin aluminum film. This interpretation was questioned because of an expected difficulty of transporting and collecting hot electrons.[3] It was suggested that some other active effect might be occurring at pinholes in the thin aluminum film. Since that time investigations of these points have shown that electron mean free paths are long enough, at least in gold[4] and perhaps in aluminum,[5] to allow such a device to be built. On the other hand, it has also been found[6,7,8] that active effects can occur at pinholes or edges in devices of the type originally reported. Thus, it appears that two very similar gain mechanisms could occur in this type of device, and care must be taken to separate them. Other methods for injection of hot electrons besides tunneling have been described; these are not necessarily free from edge effects.

During the past year, Philco has investigated ways to effect such a separation of edge and hot electron effects, using the following criteria. First, the pinhole effect device (or edge effect device) can be active regardless of the polarity of the emitter-base voltage, whereas a hot electron device can be active only when the thin base film is positive. Second, the emitter I-V characteristic of a hot electron device should be independent of the base film thickness, whereas that of a pinhole device should not, because thicker films are presumed to have fewer pinholes than thinner films. This paper describes a true hot electron device (according to these criteria).

II. CdS EMITTER STRUCTURE

The structure is similar to that previously discussed except that an evaporated layer of cadmium sulfide about 1 micron thick is deposited atop the aluminum oxide barrier in place of the gold emitter. This was used because of all emitters studied, as with present materials, it was most stable. It is not expected to have high frequency because of low density of states but it was found to be stable enough to allow characterization and it appeared not to be an edge device. Ohmic contact is made to this cadmium sulfide by means of an evaporated indium layer. Figure 1 shows a cross sectional view of this structure. In the fabrication process, a blank of germanium (1 ohm-cm, 110 orientation) 0.125 x 0.185 x 0.020 inch is chemically etched in 10-3-3 HNO_3, HAc, HF then mounted in the evaporation system. Aluminum is evaporated from a tungsten coil at a pressure of 5×10^{-6} mm Hg at a deposition rate of approximately 1000 Å/sec. Aluminum films deposited in this fashion have been found to have bulk properties down to 300 to 500 Å, as shown in Figure 2. The aluminum is oxidized at room temperature in ambient air for various times. Cadmium sulfide is then evaporated over the aluminum oxide from a molybdenum boat at a deposition rate of 1 micron per hour to a thickness of about 1 micron, film thickness and deposition rate being monitored during deposition. Indium is then evaporated over the cadmium sulfide to provide an ohmic contact. Contact is made to the indium and to the aluminum base layer with silver paste. The diodes used in this study were made by a similar process. This produces an accumulation layer emitter which allows tunneling into the aluminum base layer. Triodes using such emitters have given

$$R_{in} \sim 100\ \Omega,$$

$$R_o \sim 0.5\ M\Omega,$$

$$\alpha \sim 0.6,$$

$$h_{12} \leq 0.005,$$

$$P.G. = 500.$$

III. ELECTRICAL CHARACTERISTICS

A. Capacitance

The small signal ($\sim$ 1 mv) capacitance of CdS-Al_2O_3-Al structures of this type, where the Al film is about 1000 Å thick, has been measured at

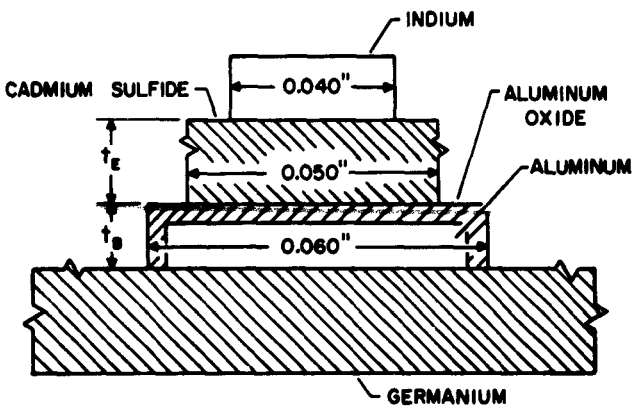

FIGURE I SCHEMATIC OF METAL INTERFACE AMPLIFIER STRUCTURE

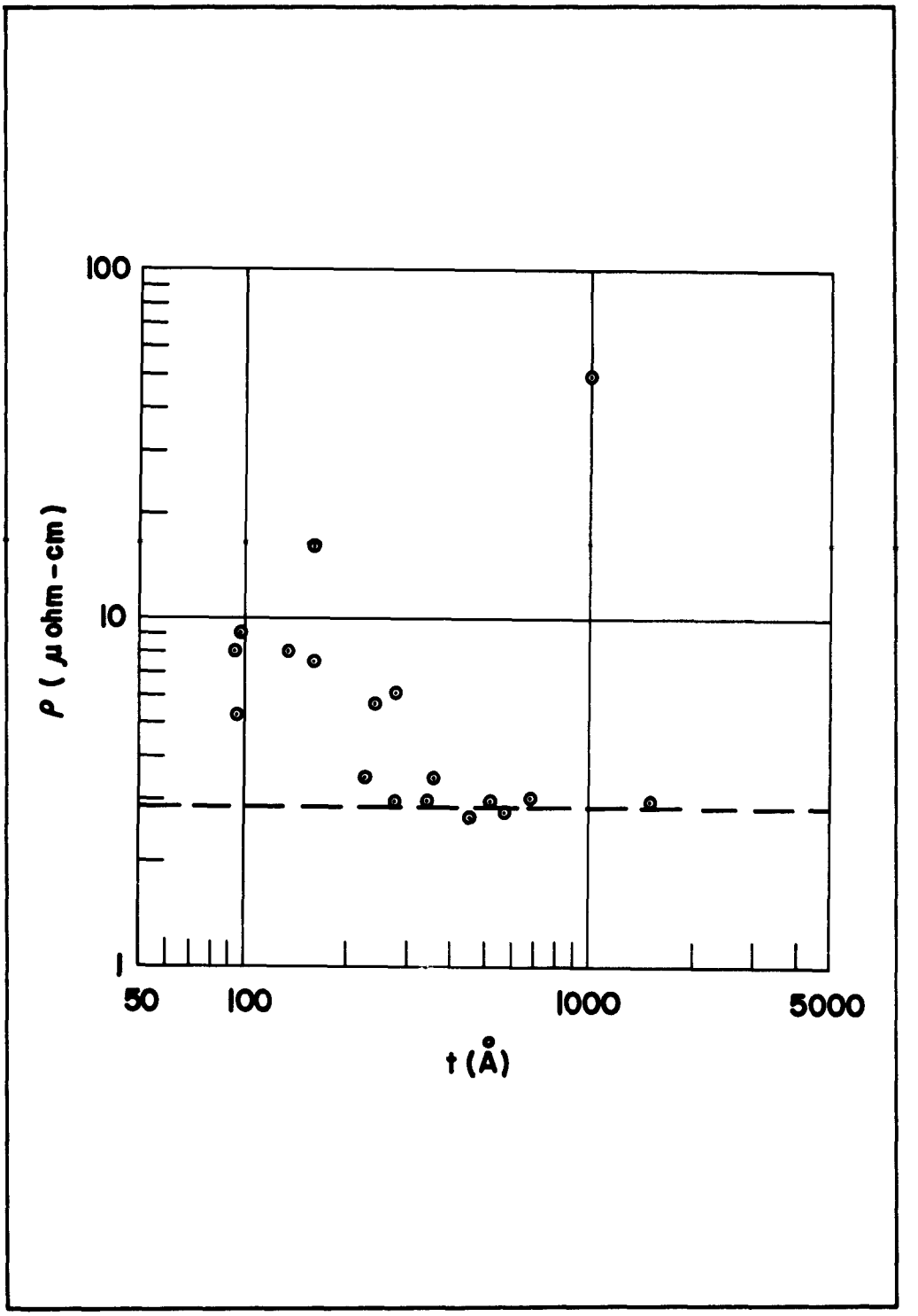

FIGURE 2 RESISTIVITY OF ALUMINUM FILMS VERSUS THICKNESS

600 kc on a Type 601 Wayne-Kerr Impedance Bridge. Typical results, shown in Figure 3, are indicative of accumulation-depletion effects at the CdS-Al_2O_3 interface. The effective barrier thickness, d/K_1, is shown to be 7 angstroms at zero bias and to vary by about $\pm$ 20 percent for bias voltages of $\pm$ 1 volt. This variation is not enough to give quantitative information on the nature of the barrier, and breakdown limitations prevented getting data over a wider voltage range. Similar data on the emitter barriers of active triodes have given the same C/A within $\pm$ 20 percent. Therefore, an upper limit of about 20 percent can be put on the portion of the base film area actually occupied by pinholes. Thus the CdS-Al_2O_3-Al structure offers the thin barrier necessary for tunneling into the Al base film.

B. I-V Characteristics

1. Emitter

The I-V characteristics of a typical emitter are shown in Figure 4. These emitters have been found to be exponential over a temperature range from room temperature to 77°K. The coefficient of the exponent and the I_o term are shown versus temperature in Figure 5. This behavior is indicative of tunneling into the aluminum, but the complicated nature of the structure makes detailed analysis of the emitter I-V characteristic quite difficult. To help in this analysis, barrier heights are now being measured; however, these data are unavailable at the present time.

The effect of aluminum film thickness on the I-V characteristic of CdS-Al_2O_3-Al diodes was studied to establish whether or not any substantial portion of the emitter current could be flowing directly into the germanium, as would be the case in an edge device. Since capacity and resistivity data indicate that pinholes account for no more than 10 to 20 percent of the film area even for the thinnest films, decreasing the number of pinholes (e.g., by making films thicker) would be expected to cause an increase in diode impedance if pinholes account for any substantial portion of the input current. Ten diodes were fabricated on germanium substrates, five having "thin" bases ($\sim$ 200 Å) and five "thick" bases ($\sim$ 1000 Å). Although the pinhole density should be substantially different for these two groups, their impedances were essentially the same - within $\pm$ 50 percent spread within each group. It would therefore appear that the film thickness (and hence the pinhole count) does not affect the diode I-V characteristic within the spread encountered for a given Al film thickness.

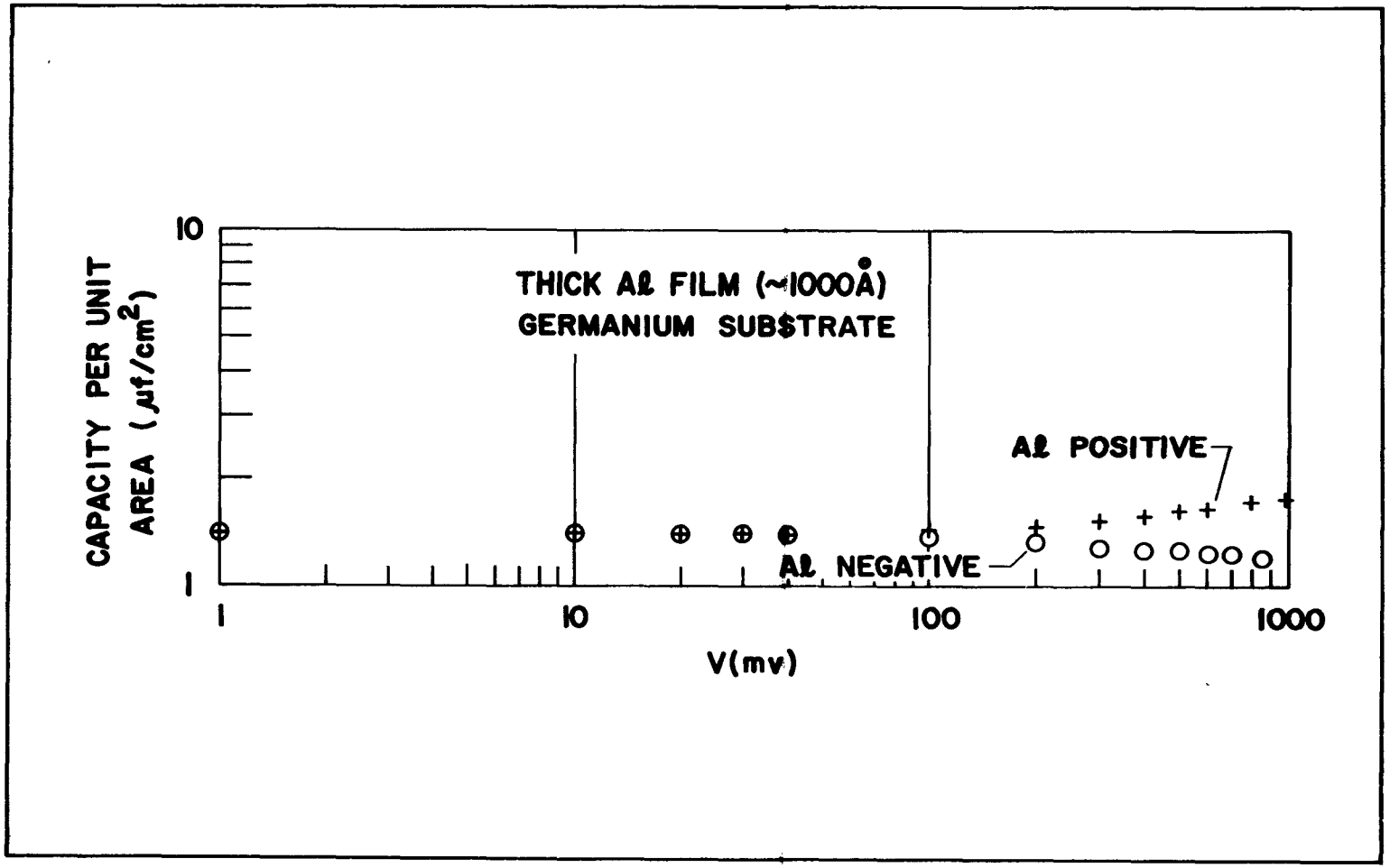

FIGURE 3 CAPACITY PER UNIT AREA VERSUS VOLTAGE OF CdS-$A\ell_2O_3$-Aℓ DIODE

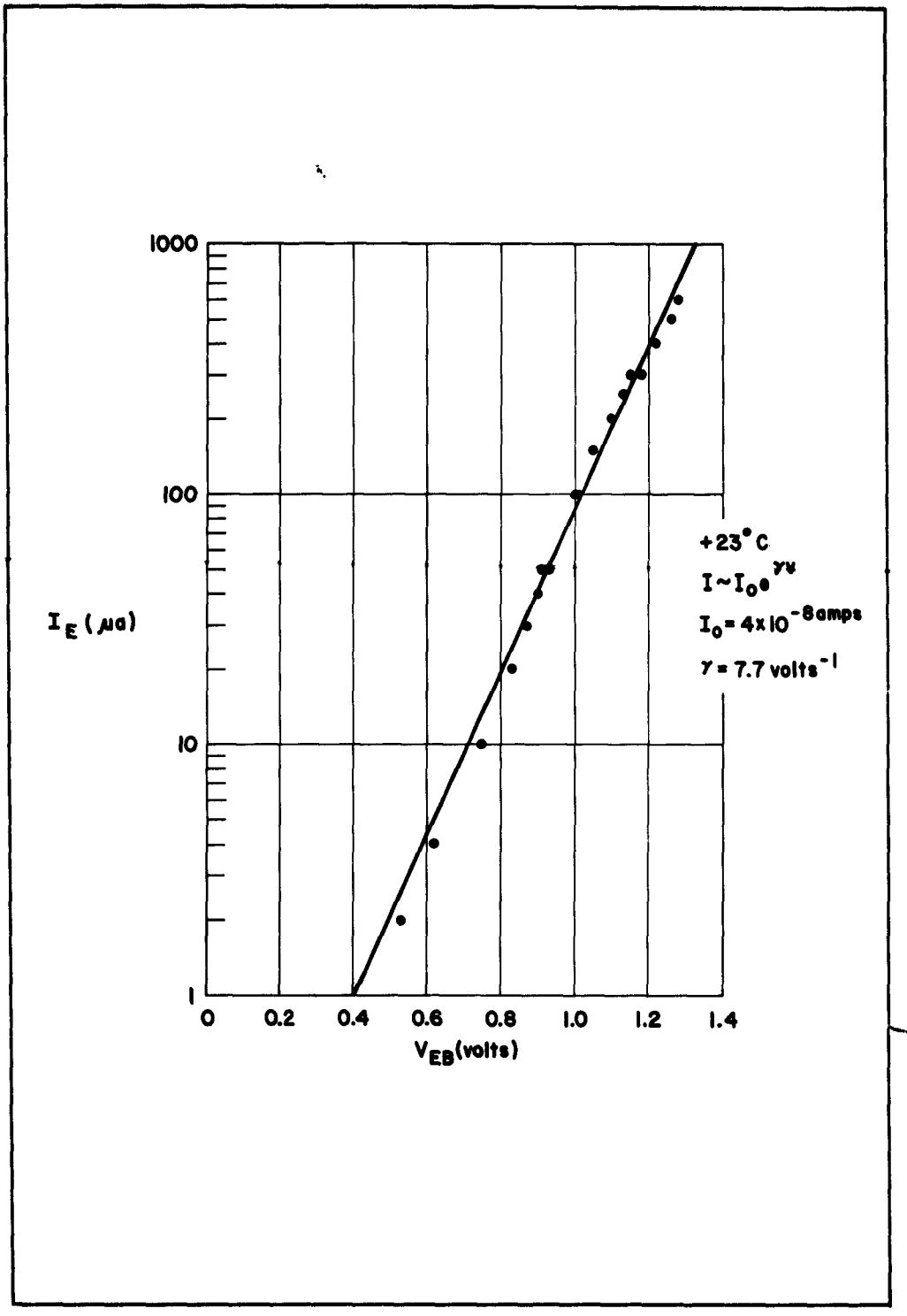

FIGURE 4 $I_E - V_{EB}$ CHARACTERISTIC OF CdS-Aℓ_2O_3-Aℓ-Ge STRUCTURE

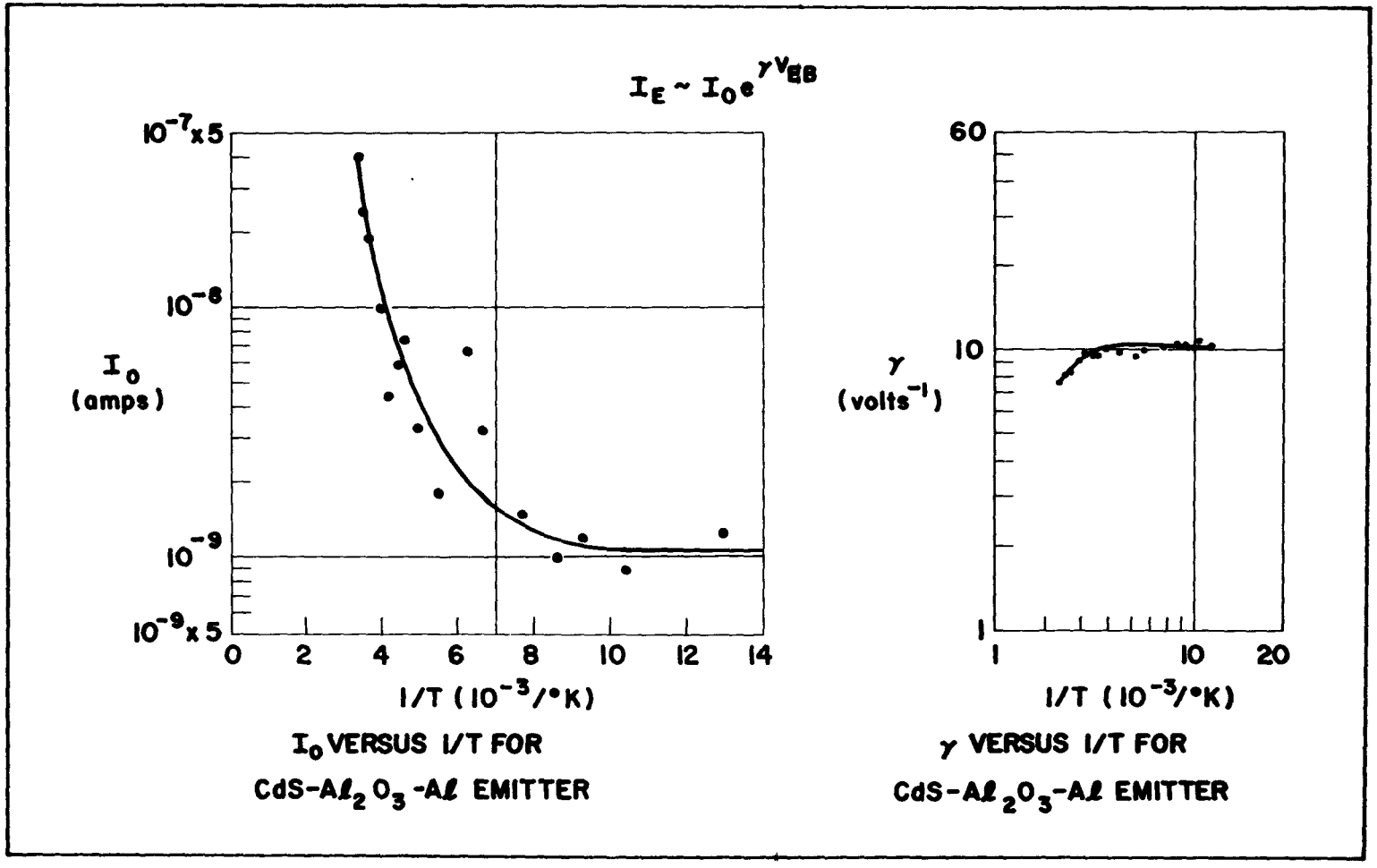

FIGURE 5 TEMPERATURE DEPENDENCE EMITTER I-V CHARACTERISTICS OF CdS-Al_2O_3-Al-Ge STRUCTURES

2. Collector

The collector current of the triode of Figure 4 was measured versus temperature. At room temperature, α_{CB} increases with I_E, saturating at high I_E; Figure 6 shows a typical plot of I_C versus I_E obtained at low temperature. Here the constant nature of α_{CB} over almost three decades of I_E indicates that no space charge limitation effects are affecting current gain. Some slight changes in α_{CB} with temperature were observed, as in Figure 7, but the significance of these changes is not yet known. They may be tied in with changes of the input I-V characteristic at these same temperatures.

In investigating the dependence of α_{CB} at room temperature on the thickness of the aluminum base layer, it has been found that, in general, α_{CB} decreases with increasing t_B. Figure 8 shows this effect. Although a large spread is seen in these data, the general tendency is obvious.

No information on collector-base barrier height could be obtained in these experiments, since very little variation was seen in the onset of emitter current. Only if substantial emitter current flows for values of V_{EB} less than the barrier height ϕ can the onset of collection be used to determine ϕ.

The effect on the gain of this structure of reversing the polarity of the emitter base voltage was checked on several dozen units. Approximately 80 percent of these showed no detectable active behavior in the so-called "reverse" direction (Al negative with respect to CdS); the remaining 20 percent showed some slight "reversibility." When an edge was intentionally introduced by allowing the CdS to overlap the Al base layer, three out of three units so built showed reversibility. Since reversibility can occur, its absence in the large majority of devices is more significant.

C. Frequency Characteristics

Examination of the frequency characteristics of structures of this type showed that the dominant time constant was the emitter base time constant. This time constant decreased with increasing emitter current. Figure 9 shows Real α versus Imaginary α for various emitter currents for one such structure, clearly exhibiting the increase in α with I_E at low currents and increase in f_α with I_E. α was found to be independent of V_{CB} over the range 0.5 to 3.0 volts. A lower input impedance unit was observed to vary in oscillating frequency from about 100 kc at 0.5 ma to 1.5 Mc at 5 ma I_E.

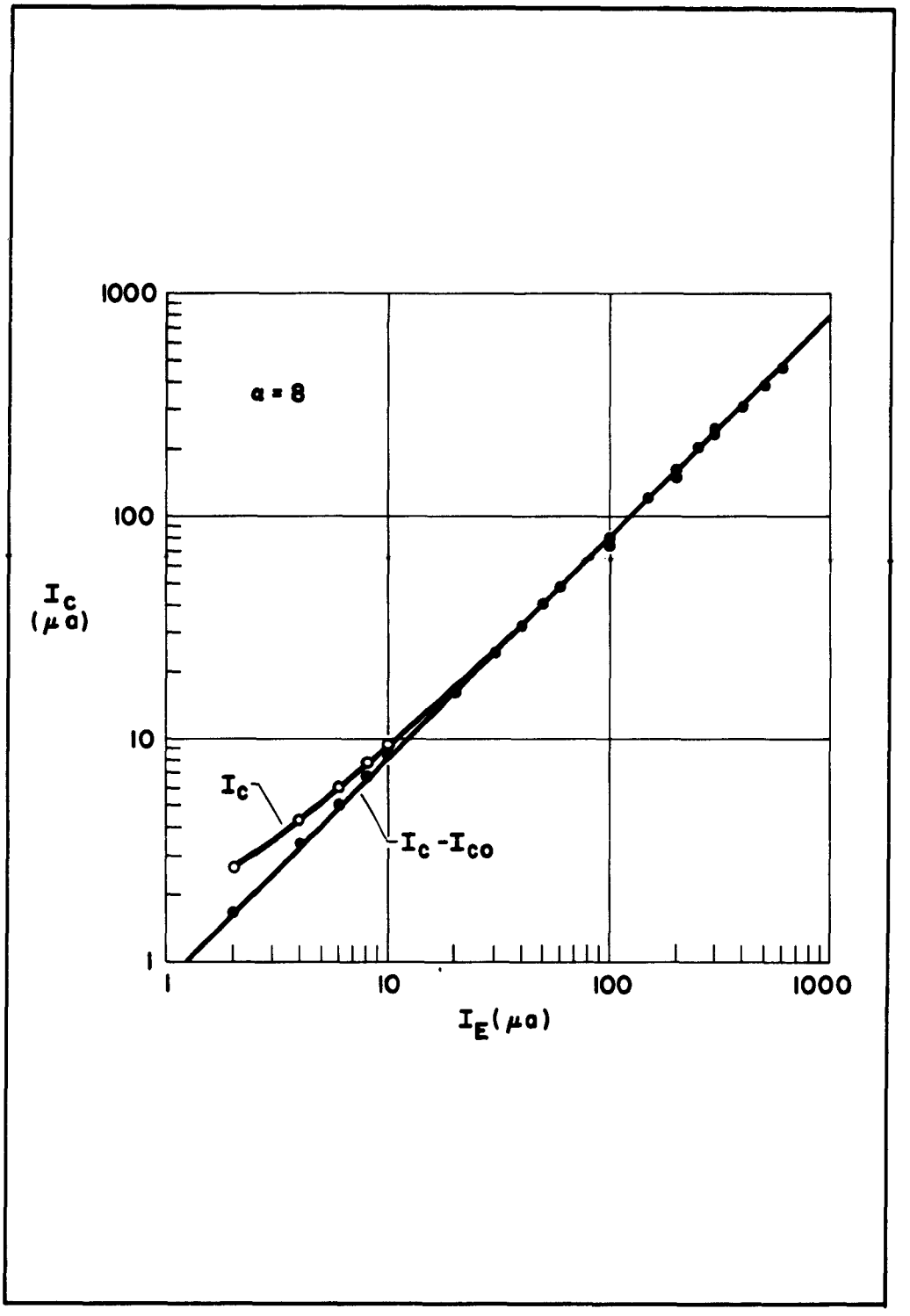

FIGURE 6 I_C VERSUS I_E FOR CdS-$A\ell_2O_3$-$A\ell$-Ge STRUCTURE

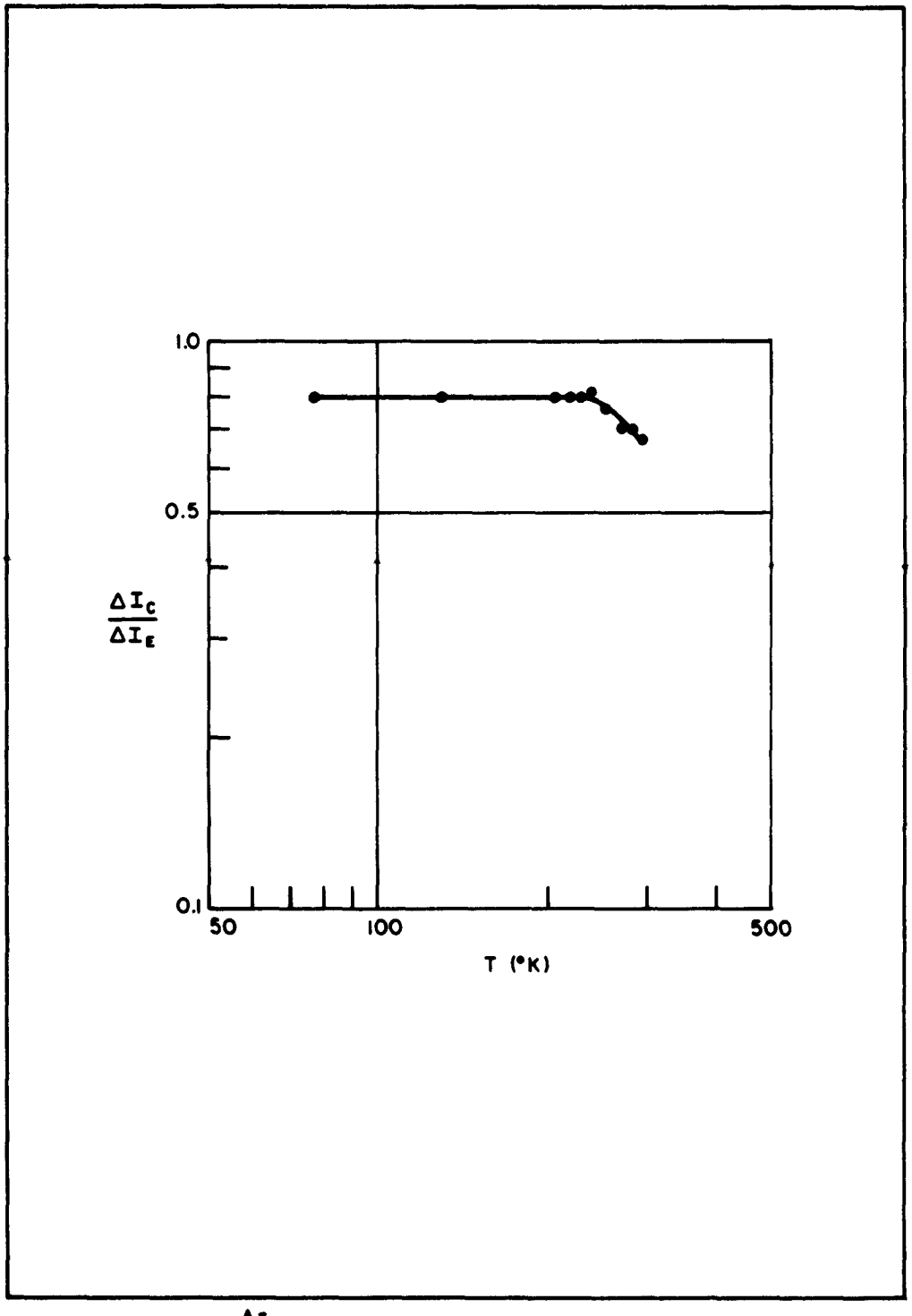

FIGURE 7 $\frac{\Delta I_C}{\Delta I_E}$ VERSUS TEMPERATURE FOR M.I.A. TRIODE

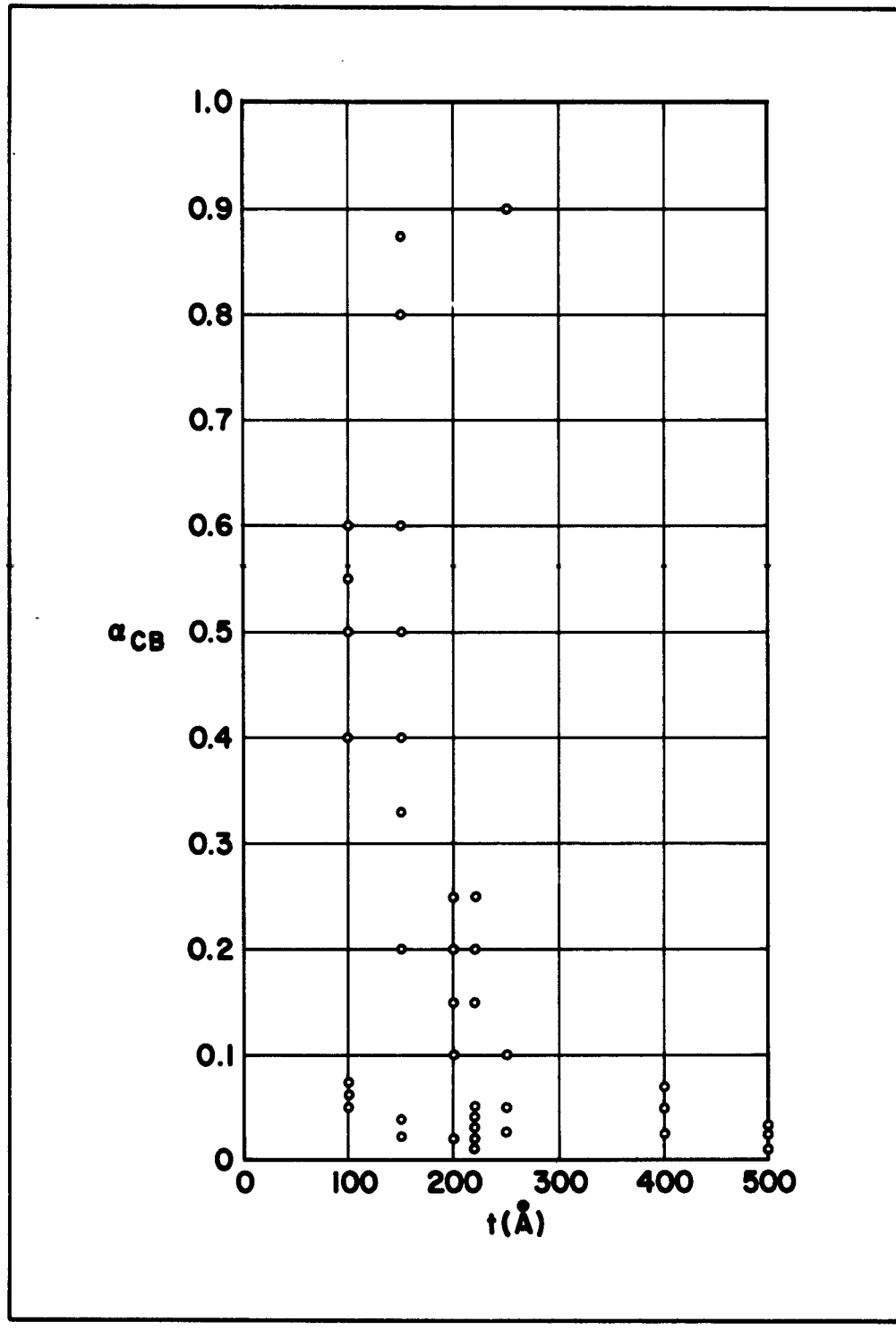

FIGURE 8 α_{CB} VERSUS Aℓ FILM THICKNESS FOR CdS-Aℓ_2O_3-Aℓ-Ge DEVICES

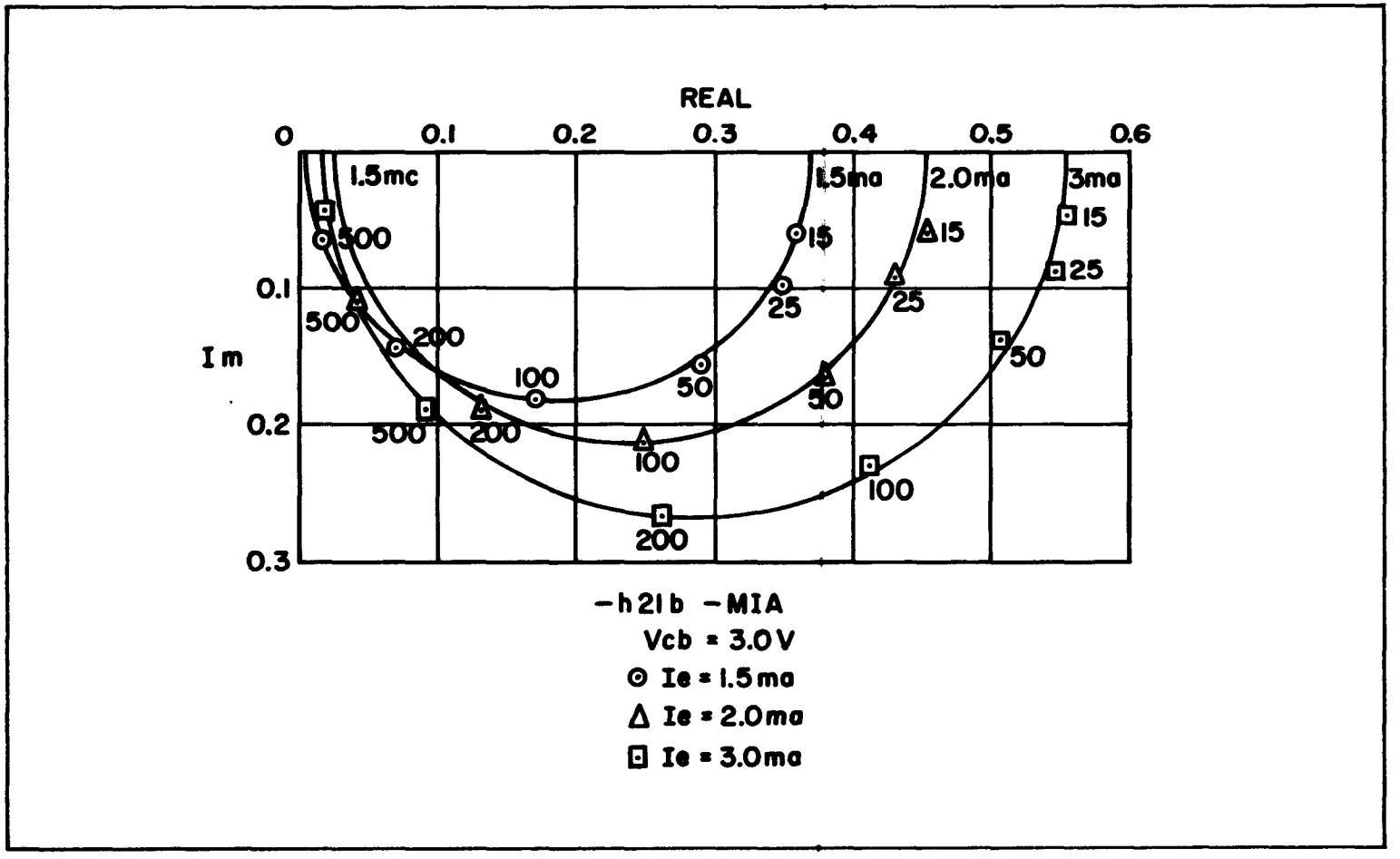

FIGURE 9 THE REAL PART OF α VERSUS THE IMAGINARY PART OF α FOR VARIOUS CURRENT LEVELS FOR METAL INTERFACE AMPLIFIERS

IV. CONCLUSIONS

A device having all the characteristics expected of a hot electron device and which is felt cannot be explained by any other mechanism, including edge emission, has been built.

V. REFERENCES

1. Spratt, Schwarz and Kane, Phys. Rev. Letters, Vol. 6, No. 7, p. 341, April 1, 1961.

2. Spratt, Schwarz and Kane, Paper presented at Solid State Device Research Conf., Stanford University, June 1961.

3. Hall, Solid State Electronics, Vol. 3, p. 320, November-December 1961.

4. Spitzer, Crowell, and Attalla, Phys. Rev. Letters, Vol. 8, No. 2, p. 57, January 15, 1961.

5. Quinn, Phys. Rev., Vol. 126, No. 4, p. 1453, May 15, 1962.

6. Spratt and Schwarz, Paper presented at Hot Electron Symposium, Philco Scientific Laboratory, February 1962.

7. Schwarz and Spratt, Proceedings IRE, Vol. 50, No. 4, Part 1, p. 467, April 1962.

8. Lavine and Iannini, Solid State Electronics, Vol. 5, p. 109, March - April 1962.

APPENDIX B*

Application of Mercury Microprobe Scanning System to Measurement of Discontinuity and I-V Characteristics in Thin Oxide Films

S. S. Choi

Philco Corporation
Scientific Laboratory
Blue Bell, Pennsylvania

A portion of this paper was presented at the Electrochemical Society Spring meeting, April 15-18, 1963, Pittsburgh, Pa.

Introduction

The great interest in thin film microelectronics has focused attention on the properties of thin layers of various materials. Thin insulating oxide films, in particular, are being studied for use in active devices, in capacitors, and for isolation purposes. In many of these applications it is desirable to have such insulating films as thin as possible and still retain electrical isolation. In practice, one is often prevented from using very thin films due to the fact that defects may occur which result in performance degradation or give nonreproducible experimental results leading to misleading interpretations. It is, therefore, necessary to minimize such defects, but this requires that they be detected and characterized. The defects of interest may sometimes be detected by optical techniques or by electron microscopy, but such techniques cannot be used to study all electrical discontinuities of interest. These defects are often referred to as pinholes, cracks, fissures,

* The work described in this paper represents Philco-supported work in the general area of interest to the subject contract.

microfissures, pores, impurities or crystalline sites in dealing with amorphous films depending on the mechanism of formation. However, in this paper such defects are referred to as simply pinholes or discontinuities.

Applications

Apparatus

A simple mercury microprobe and scanning system were developed[1] and utilized to detect pinholes and other localized imperfections in thin oxide insulating films and to evaluate them as a function of process technology. Problems of pressure contacts and film scratches were thereby avoided. Relatively high resolution is obtainable since the probe contact area can be controlled to less than 10^{-6} cm^2.

Figure 1 shows one type of mercury microprobe. It is constructed in such a way that the capillary portion (see Figure 1) of the probe can be easily interchanged with different size capillaries so as to give large flexibility of the contact area. Because the distance between the sample and the capillary is often required to be very short, the end of the capillary should be cut very flat to avoid scratching the sample surface. It is important, when mercury is introduced into a syringe, to eliminate air pockets between the mercury and the piston in order to control precisely the size of the mercury ball on the tip of the capillary.

---

1) Details of the probe and scanning system will be published separately.

microfissures, pores, impurities or crystalline sites in dealing with amorphous films depending on the mechanism of formation. However, in this paper such defects are referred to as simply pinholes or discontinuities.

Applications

Apparatus

A simple mercury microprobe and scanning system were developed[1] and utilized to detect pinholes and other localized imperfections in thin oxide insulating films and to evaluate them as a function of process technology. Problems of pressure contacts and film scratches were thereby avoided. Relatively high resolution is obtainable since the probe contact area can be controlled to less than 10^{-6} cm^2.

Figure 1 shows one type of mercury microprobe. It is constructed in such a way that the capillary portion (see Figure 1) of the probe can be easily interchanged with different size capillaries so as to give large flexibility of the contact area. Because the distance between the sample and the capillary is often required to be very short, the end of the capillary should be cut very flat to avoid scratching the sample surface. It is important, when mercury is introduced into a syringe, to eliminate air pockets between the mercury and the piston in order to control precisely the size of the mercury ball on the tip of the capillary.

1). Details of the probe and scanning system will be published separately.

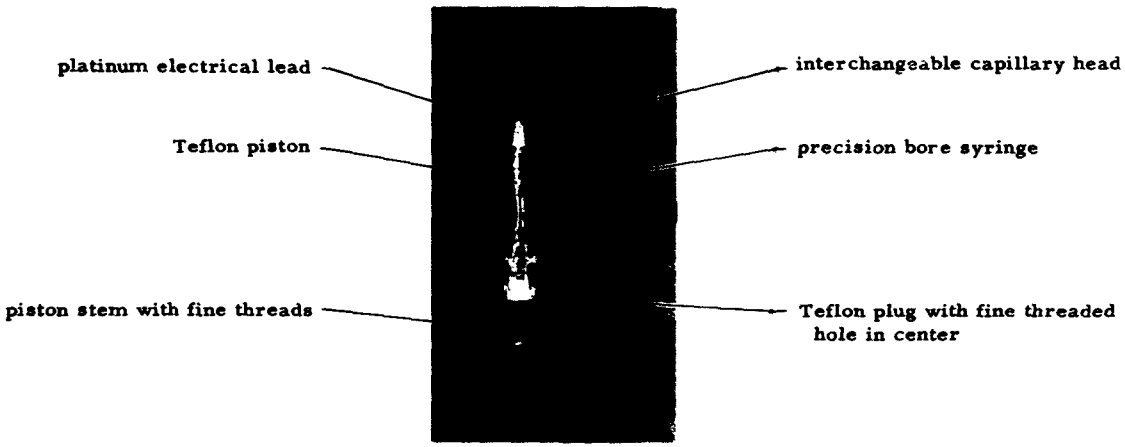

Figure 1 Mercury Microprobe

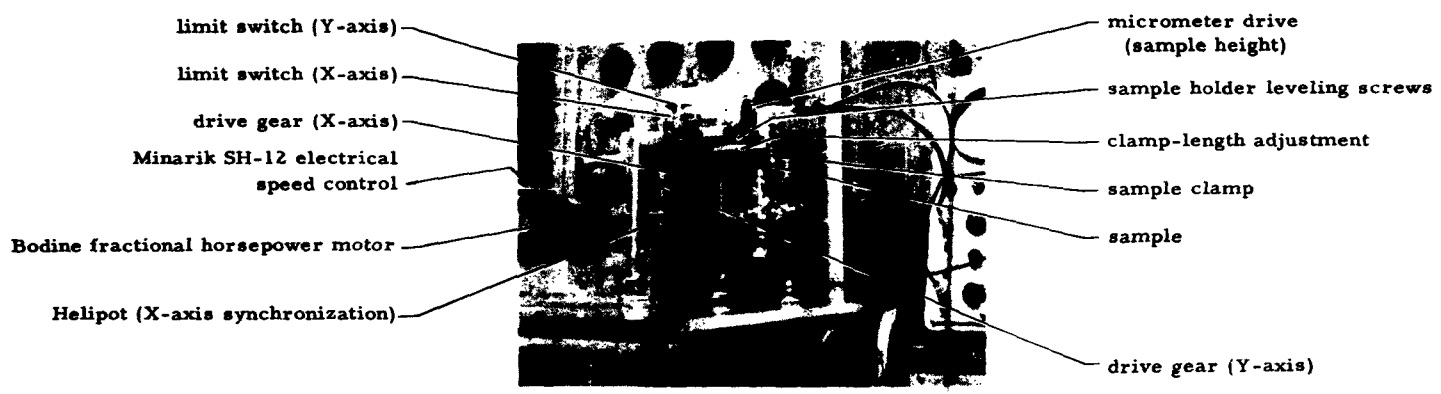

Figure 2 Mercury Probe Scanning System

Figure 2 shows the scanning system without optical microscope. The sample should be clamped horizontally by checking with an optical microscope. Some of the circuit diagrams of the arrangement are shown in Figure 3.

With such an arrangement, one can measure the electrical characteristics of particular spots on a sample or scan the entire sample with a given voltage applied to detect the regions of low dielectric strength by current modulation of the Z axis on a tektronix 536.

Measurement of Discontinuities

Figures 4 and 5 show some of the photographs taken by scanning the sample surface with the microprobe. The samples used for these photographs were prepared by anodizing tantalum films which had been sputtered on glass slides.* No visible surface wetting by the mercury was observed on tantalum oxide, or on any other oxide tested which had a standard free energy of oxide formation more negative than HgO (red).

In Figures 4 and 5, the bright spots are the conductive region; the absence of a trace indicates a lack of conductive or breakdown region at the applied voltage shown. It can be noticed that the intensity of the trace is increased with increasing bias at a given spot. It should also be noticed from Figure 4 that the pattern of the pinhole distribution is the same in (b) and (c), although more defects are seen in (c) due to higher bias. However,

* Some of the parameters and conditions for the preparations of the samples used are given in Appendix A and B.

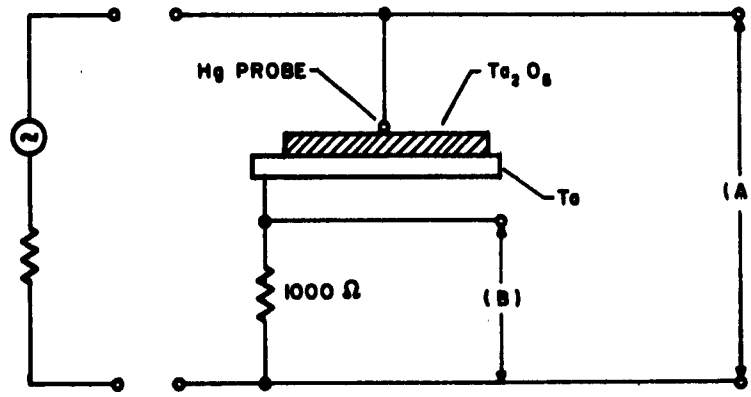

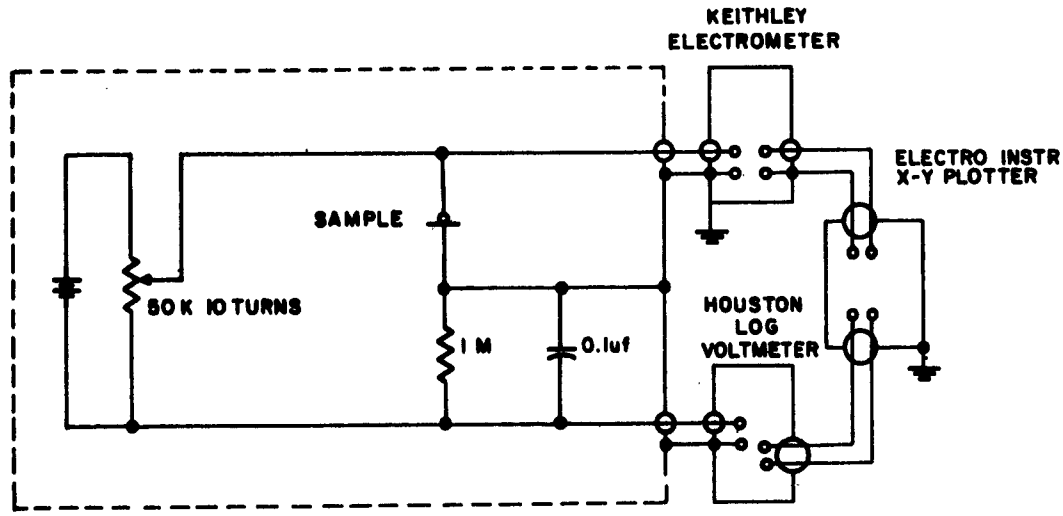

Figure 3 Circuit Diagrams

(a)

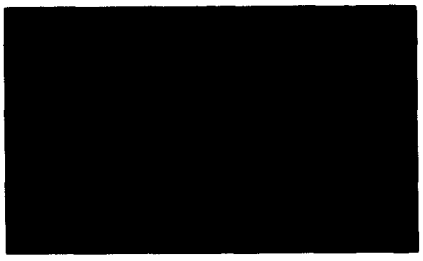

Hg : Positive
X : 1 in/min
Y : ~1 mm/step
Ta_2O_5 ~ 800Å

Applied Bias: 4.0 volts d.c.

Note: Probe purposely shorted to produce single dot on photo at end of analysis

(b)

Applied Bias: 8.5 volts d.c.

(c)

Applied Bias: 9.5 volts d.c.

X-axis scanning rate = one inch per minute; Y-axis = approximately one millimeter steps. Ta film thickness: 2500 Å deposited at 300 Å per minute; formation voltage: 40 volts (800 Å); Hg electrode positive biased.

Figure 4 Pinholes Detected in Anodized Ta

* Note: Previous breakdown work had been performed on this sample

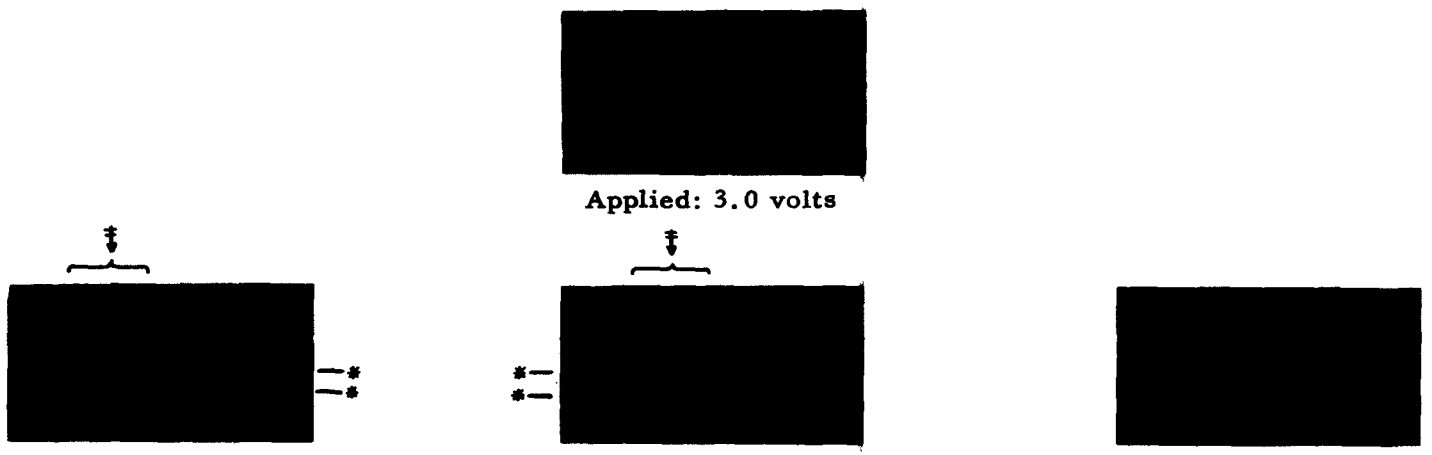

Note: This profile taken 2nd in the series 2.0-1.5-2.5-3.0 volts there is indication of healing

Note: Lowest trace subjected to 3.0 volts for one scan when determining suitable voltage for this profile. Voltage was then reduced to 2.5 volts.

Figure 5 Pinhole Profile with DC Voltage

when the same line was repeatedly scanned with decreasing voltage, some spots either showed decreased intensity or disappeared altogether (see Figure 5 ↓), indicating that the breakdown is nondestructive in some cases. Thus, distribution of such defects (from the electrical point of view) is also a function of applied voltages with this technique. However, at the point where the destructive breakdown occurred, the trace always appeared with maximum intensity at any bias.

It is clear from these photographs that the pinhole distribution is not uniform throughout the whole sample area, therefore it is difficult to define a meaningful "average pinhole density" (pinholes/cm^2, etc.).

One interesting phenomenon observed was that some spots drew less current or disappeared with additional bias. This phenomenon was observed only with silicon monoxide films which were evaporated on sputtered tantalum film. These spots usually show abnormal I-V characteristics. I-V characteristics traced on some of these spots are shown in Figures 6 and 7, which indicate the existence of negative resistance regions in such samples. As can be seen from these figures, the I-V characteristic is repeatable with the peak current always occurring at 6 volts. However, not all such spots are stable; some are unstable and erratic. Such an example is shown in Figure 8 for comparison. When carefully examined, the region of the film in which such spots occur sometimes shows slight differences in color when viewed with the naked eye. The comparison of electron micrographs and

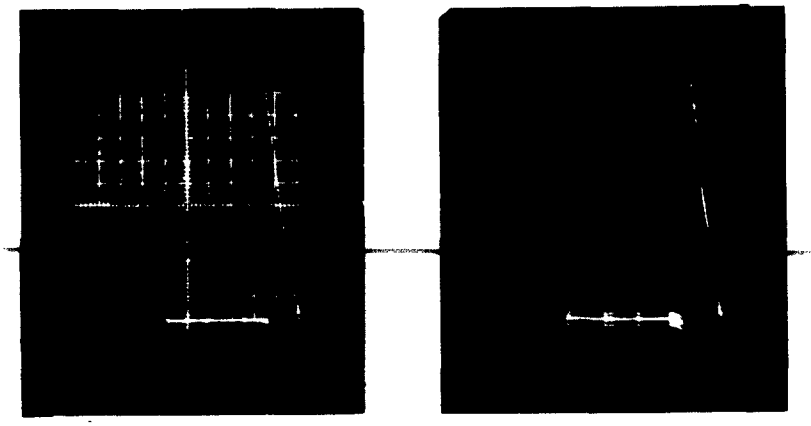

VERT 1μa/cm
HORIZ 5.0v/cm

HORIZ 5.0v/cm
VERT 1μa/cm

SiO Film Thickness: 800 Å

Figure 6 Abnormal I-V Characteristic of SiO on Ta

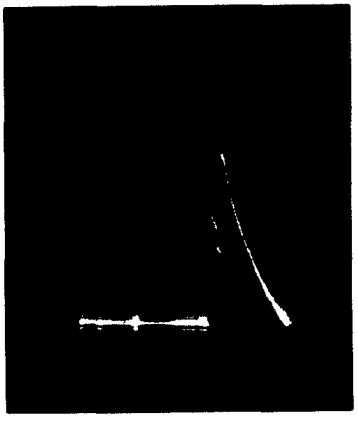

HORIZ 2.0v/cm
VERT 10μa/cm

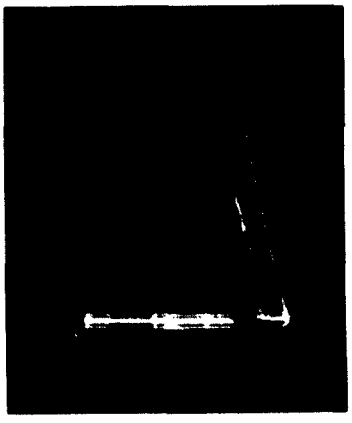

HORIZ 2.0v/cm
VERT 1μa/cm
Note: Large peak
voltage → 0

SiO Film Thickness: 800 Å

Figure 7 Abnormal I-V Characteristic of SiO on Ta

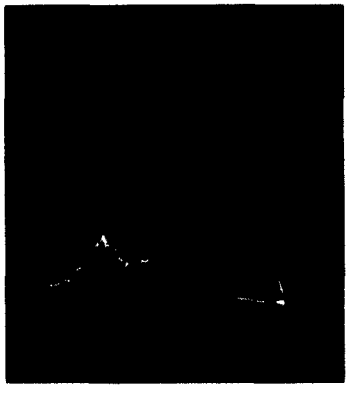

50μa/DIV VERT AXIS
0.2v/DIV HORIZ AXIS

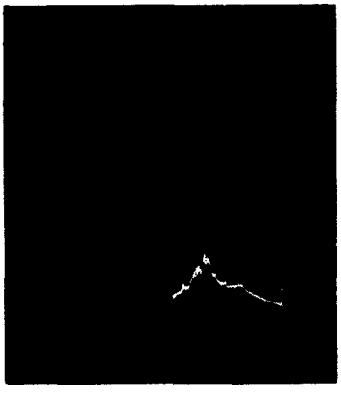

50μa/DIV VERT AXIS
0.5v/DIV HORIZ AXIS

SiO ON GOLD - 100Å
(+) Au-SiO-Hg (-) SYSTEM

Figure 8 Unstable Abnormal I-V Characteristic of SiO on Au

X-ray diffraction of such areas, and other areas in the same sample, is also planned in order to study the cause of such abnormal I-V characteristics.

In an attempt to obtain better resolution of pinholes, and to study the reproducibility of this technique, the sample was scanned with a microprobe at a given speed and with a given applied voltage, and the current drawn by the probe recorded as a function of time with a motion picture camera. When repeatedly scanned on the same place of the sample, the current was drawn exactly at the same spot. Figure 9 shows the sequence of such a sweep showing the reproducibility of this technique. The speed of the camera was 33 ft/min, and that of the sample was 1 in/min.

Measurement of I-V Characteristics

With this microprobe, I-V characteristics of several samples of different material were measured.

In measuring the I-V characteristics and dielectric strength of the sample, the diameter of the contact area was approximately 10 mils. With the system $Ta/Ta_2O_5/Hg$, strong rectification was observed throughout the whole sample surface. Easy direction of current flow is the forward direction, (Hg positive). Even with a very small contact area (diameter of contact area less than 0.5 mil), such rectification phenomena did not disappear. Thus, the results observed here are contradictory with the published

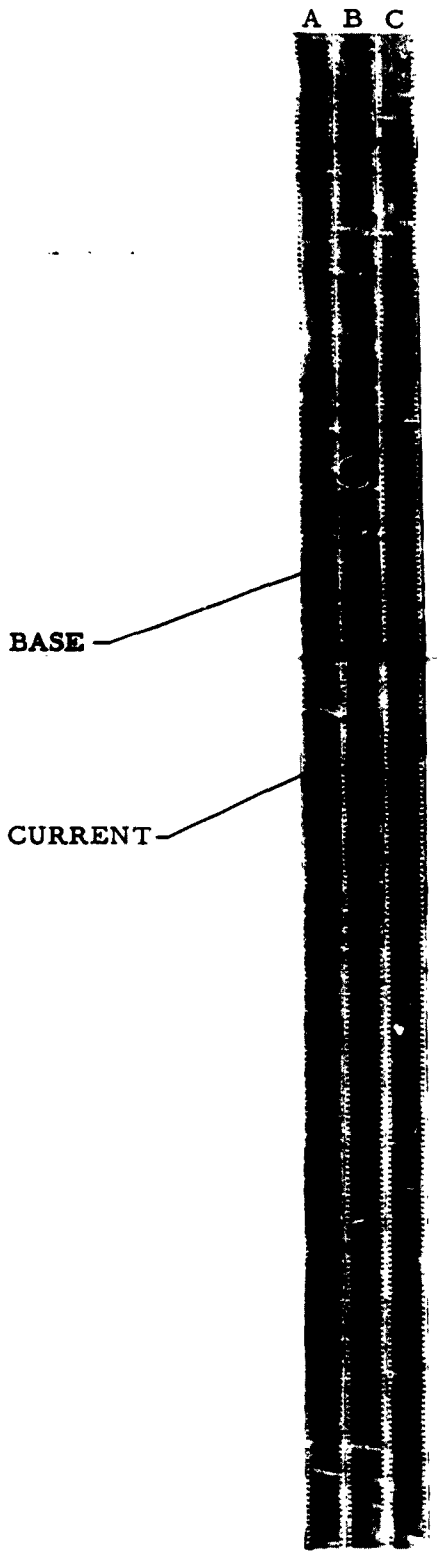

Figure 9 Sequence of Pinhole Detections (Total film length: 30 feet) (Corresponds to sample length of ≈ 1 in.) Film length shown: 4 :

postulation that rectification in the system like Ta/Ta_2O_5/metal occurs at singularities,[2,3] but is consistent with the statement of Winkel et. al.[4] However, in the case of evaporated SiO on sputtered tantalum films, no such phenomena was observed. Figure 10 shows the I-V characteristics of $Ta/Ta_2O_5/Hg$ with an a. c. sinewave applied; Figure 11 shows I-V characteristics of the system Ta/SiO/Hg showing symmetrical I-V characteristics. I-V characteristics of the system $Ta/Ta_2O_5/Hg$ were measured with forward direction on several different thicknesses of oxide and the log I vs. voltage curve has two distinctive curvatures in the current region 10^{-9} to 10^{-5} amperes. When log I is plotted against $V^{1/2}$, two parts of the curve become straight lines as shown in Figure 12. As can be seen from this figure, the slope of each part of the plot differs but the current value at which these two straight lines meet is almost constant regardless of the oxide thickness. When log I is plotted against field (i. e., $\frac{V}{d}$), curves for thicker films (over 300 Å) overlap, and the points at which two straight lines meet in Figure 12 gives the same field value of $(1.1 \pm 0.1) \times 10^6$ V/cm regardless of the oxide thickness.

On the other hand, in the case of the system Ta/SiO/Hg, log I vs. V gives a straight line as shown in Figure 13. For comparison, the I-V

---

2) D. A. Vermilyea, J. Appl. Phys, 27, 963 (1956).

3) J. Burnham and P. Robinson, Ann. Rep. Conf. on Electric Insulation (1948).

4) P. Winkel and B. Verkerk, Philip Res. Repts, 13, 501 (1958).

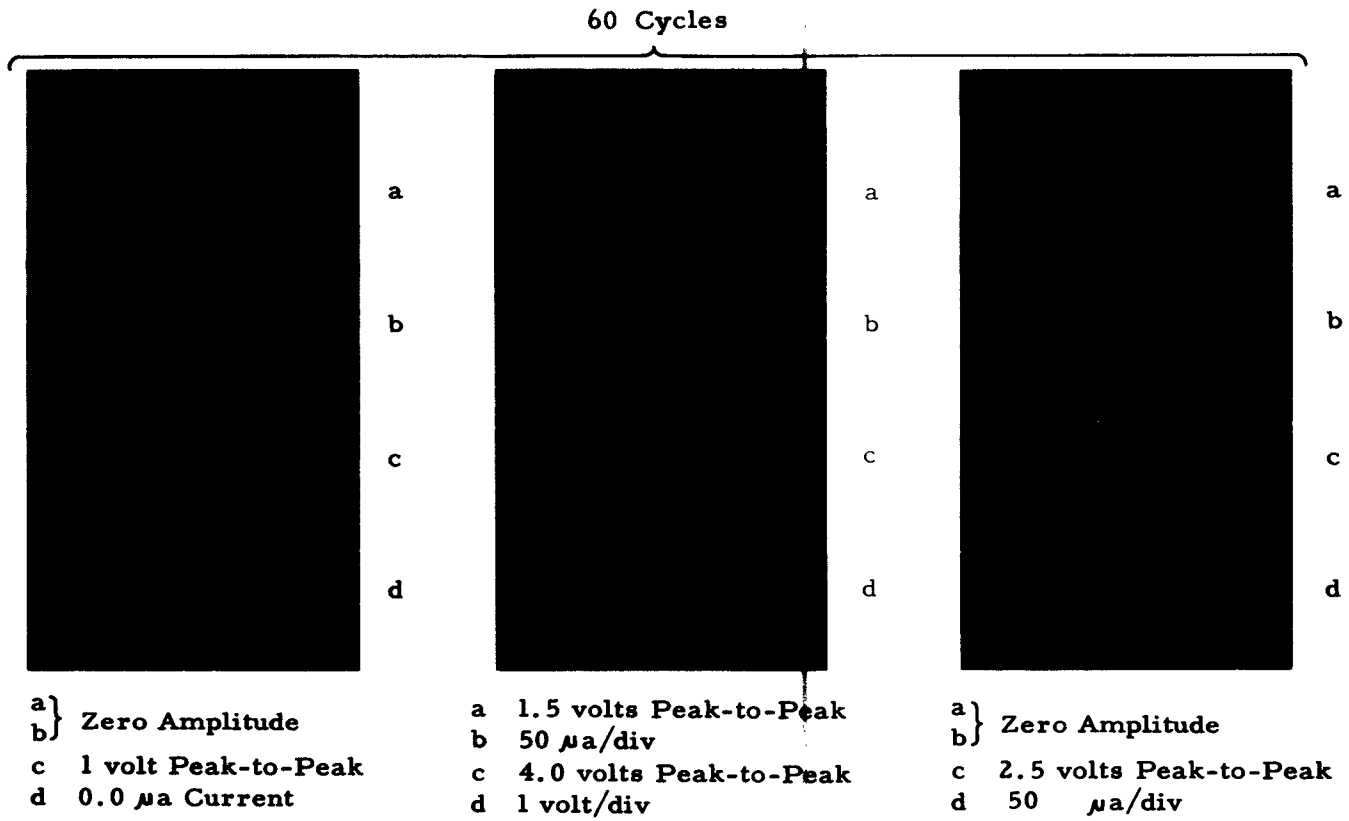

Figure 10 Rectification of Ta/Ta Oxide/Mercury System

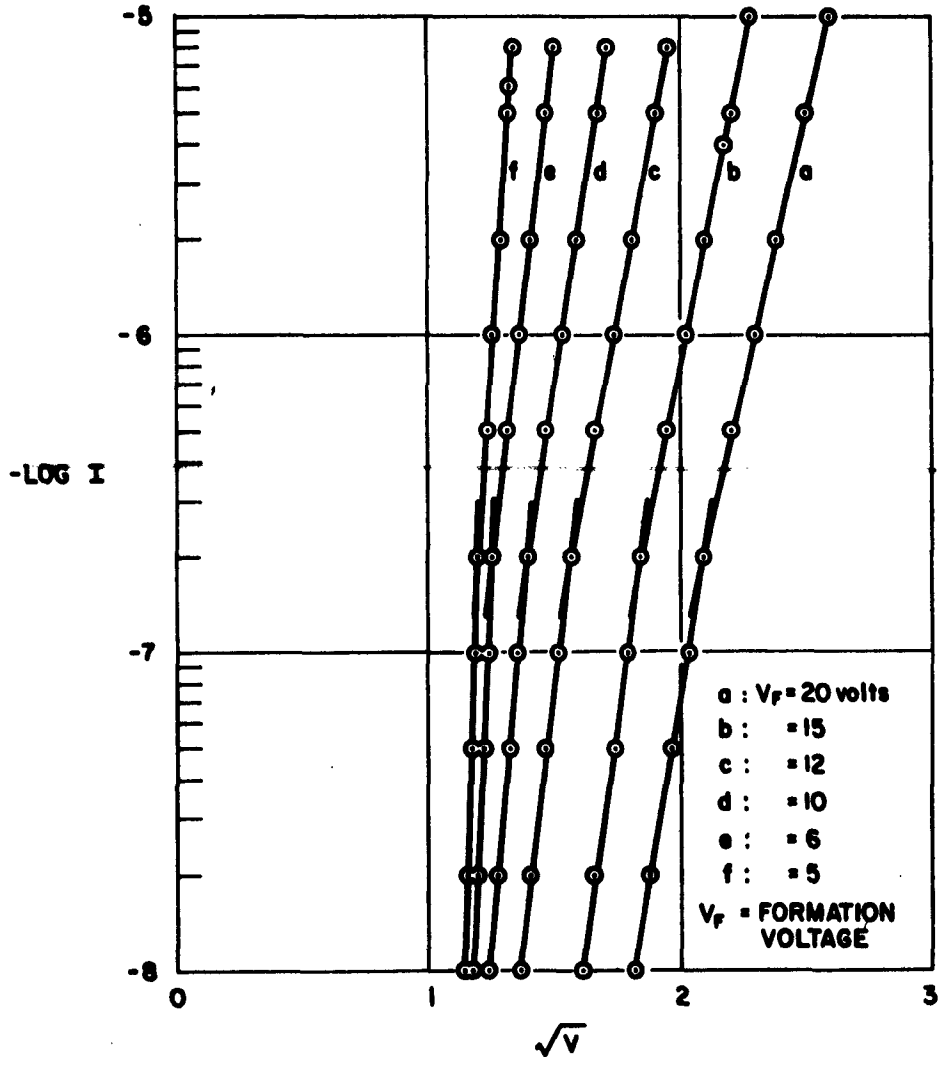

Figure 12 I-V Characteristics of Ta/Ta-Oxide (Anodized)/Hg at Various Thicknesses

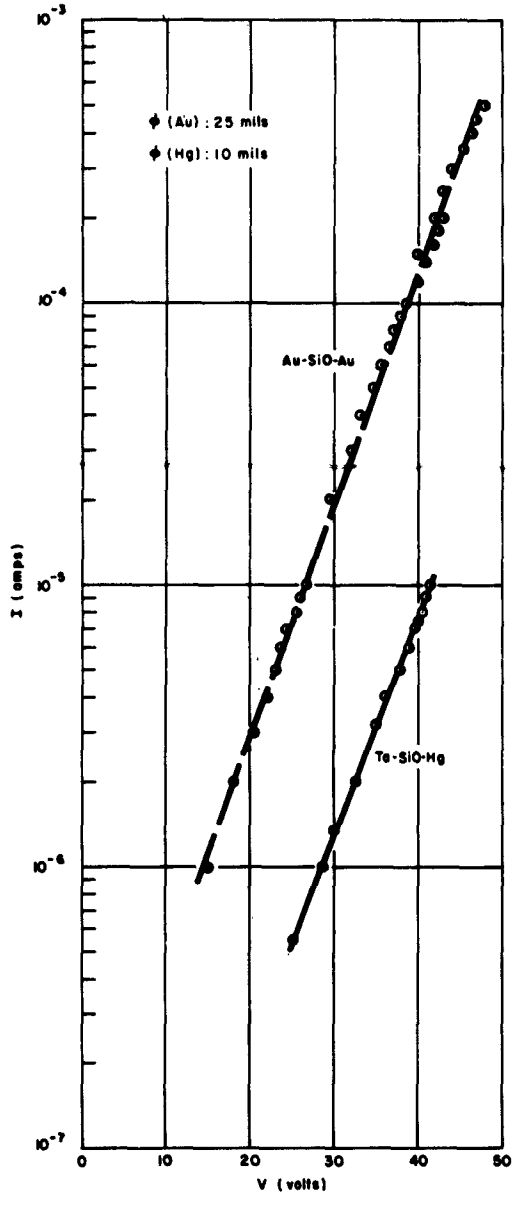

Figure 13 I-V Characteristics of Ta-SiO-Hg Diode and Au-SiO-Au Diode

characteristics of the system Au-SiO-Au are shown. It is interesting to note that the slope of the two lines are exactly the same even though line A has different base and counterelectrode metals. The diameter of the contact area for Au-SiO-Au is about 25 mils while Hg contact has less than 10 mils of contact diameter.

Measurement of Dielectric Strength

When the system Ta/Ta_2O_5/Hg draws current in the order of micro-amperes, the oxide usually breaks down.

The d. c. breakdown strength of anodized Ta_2O_5 films increases monotonically with increasing formation voltages (increasing film thickness); but the magnitude of the dielectric strength changes with the polarity of the applied voltage. With Hg negative, the breakdown voltage is about the same as the formation voltage, while with the opposite polarity, the oxide film breaks down at about half the value of that of reverse bias. Figure 14 shows the breakdown voltages of Ta_2O_5 film with forward and reverse bias versus formation voltage.

When the applied voltage is increased to the vicinity of the breakdown voltage, a sudden current flow can be observed through the oscilloscope. Instantly after breakdown of the oxide film by reducing the applied voltage, the amount of current flow also can be reduced depending upon the voltage applied.

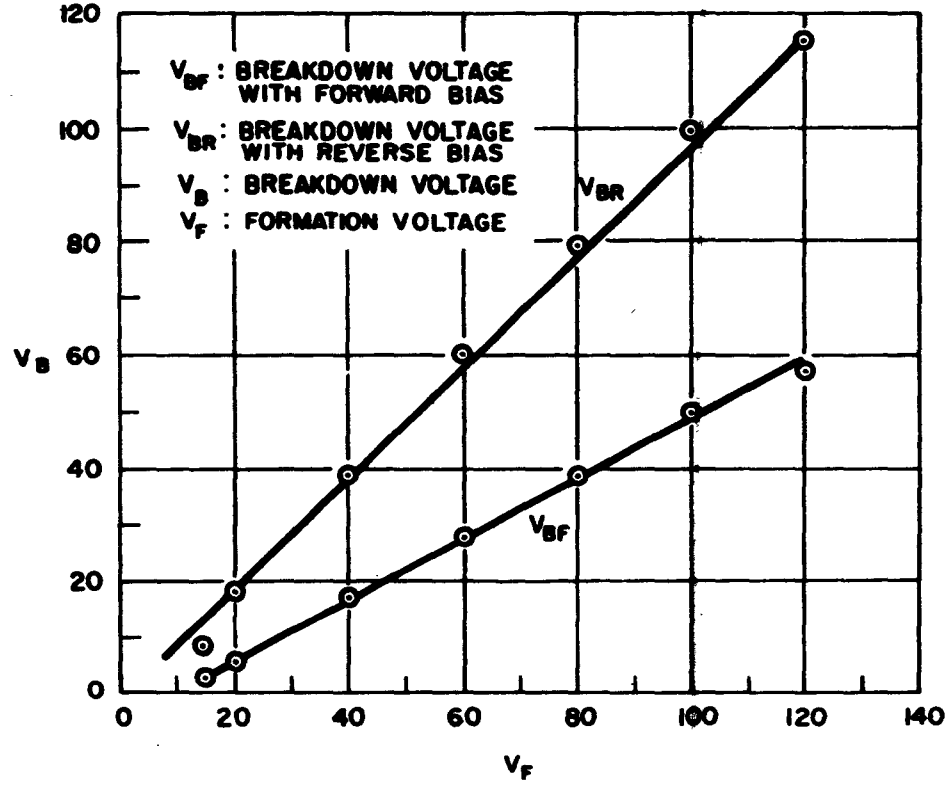

Figure 14 Breakdown Voltage of Ta_2O_5 Film Versus Formation Voltage

When the applied voltage is reduced to less than 1 volt, the current is gradually decreased to "zero"* without further reduction of the applied voltage (i. e., the oxide film healed again). At about 0.5 volts, the time to heal completely is between 30 and 60 seconds although on some occasions it took several minutes. The healing times depend on several factors, viz., the final voltage applied, the time elapsed before reducing the applied voltage after the breakdown, and the actual breakdown voltage, etc.

When the oxide film is broken at too high a voltage, or when power dissipation is continued after breakdown without reducing the applied voltage, such healing phenomena is not observed. However, when the dissipated energy is kept small, a region of the film can be repeatedly broken down and allowed to "heal," but breakdown then occurs at a lower voltage than initial breakdown. It is not clear whether ion motion plays any part in the healing although the repeated recovery and reproducibility would suggest electronic avalanche followed by lattice cooling for short pulses of energy. Table I shows I-V characteristics after healing. These data still show the rectifying properties of the films.

If instead of d. c., a pulsing voltage is used, the breakdown voltage increases depending on the pulsing conditions. Table II shows the results obtained with pulsing techniques which may give some insight into the relationship between breakdown voltage and power dissipation.

---

* Current line in the oscilloscope approach base line. It is not strictly zero current.

TABLE I
I-V CHARACTERISTICS AFTER HEALING

Polarity	Forward Biasing (Hg-positive)				Reverse Biasing (Hg-Negative)			
Area No.	1		2		5		6	
	E_v* (volts)	I (ma)	E_v (volts)	I (ma)	E_v (volts)	I (ma)	E_v (volts)	I (ma)
	0.50	0.00	0.50	0.00	0.50	0.00	0.50	0.00
	1.0	0.01	1.0	0.00	1.0	0.00	1.0	0.00
	1.5	0.02	1.5	0.01	1.5	0.00	1.5	0.00
	2.0	0.64	2.0	0.68	2.0	0.00	2.0	0.00
	2.5	1.15	2.5	1.70	2.5	0.01	2.5	0.01
	3.0	1.80	3.0	2.40	3.0	0.02	3.0	0.02
*	4.0	3.4	4.0	3.2	4.0	3.2	4.0	3.20
	5.0	3.9	5.0		5.0	4.4	5.0	4.40
	6.0	5.6	6.0	4.6	6.0	4.8	6.0	4.80
Initial Breakdown Voltage	3.2 volts		1.8 volts		5.0 volts		7.0 volts	

Formation voltage of the oxide: 10 volts
Waiting period (after heal): 2 minutes.

Pulse width: 9 μsec
Rep. rate : 5000 pps
Period : 1 min at applied voltage E

TABLE II
RELATION BETWEEN
BREAKDOWN VOLTAGE AND TOTAL PULSE TIME

Frequency x Pulse Width	E_{BF} (v)
DC	39
400×10^{-3}	46
200×10^{-3}	50
20×10^{-3}	52
4×10^{-3}	55

If a single pulse is applied to the sample, the breakdown voltage increases about two to three times that of the case of d. c. This is true with all samples tested, i. e., Ta/Ta_2O_5, Al/Al_2O_3, Ta/SiO, and Au/SiO. When the pulse amplitude is sufficiently high the oscillations occur and the current density is abnormally high. Figures 15, 16 and 17 show such oscillations with the single pulse applied to different oxides. The fact that such oscillations were observed only in oxides of thicknesses of up to 300 Å, and not in films of thickness above 500 Å, it may be concluded that these oscillations are due to the negative resistance at such high applied voltage or tunneling through the oxide films. However, the above results are preliminary in nature and are obtained under ordinary room atmospheric conditions. For further comparison, the application of this technique under reduced pressure and inert atmosphere is in progress. A systematic study is scheduled, using samples produced under different conditions and having different histories, to evaluate the observed results as a function of process technology and history. Some of the limitations of this technique and the implications of the observed results will be dealt with in a succeeding paper. To aid in the analysis of failure mechanisms of devices and to evaluate the best conditions of process technology, the above results will be incorporated with the studies of metallurgical, physical or chemical changes in sample phases, and with the behvaior of impurities under different operating conditions by adopting various techniques, including the use of radioactive isotopes and radioactivation techniques.

SINGLE PULSE 50μsec at 20v
HORIZONTAL 10μsec/cm
VERTICAL 5v/cm

200Å SiO/Ta
HORIZONTAL 10μsec/cm
VERTICAL 5ma/cm

200Å SiO/Ta
HORIZONTAL 1μsec/cm
VERTICAL 1ma/cm

Figure 15 Oscillation in SiO Film with Single Pulse

300 Å Ta_2O_5 E_f=15v
SINGLE PULSE 50μsec at 30v
MEASURING VOLTAGE ACROSS
FILM VERSUS TIME
HORIZONTAL 5μsec/cm
VERTICAL 2v/cm ZERO SUP.
OSC INCREASE WITH TIME

300 Å Ta_2O_5 1st PULSE
SINGLE PULSE 20μsec at 10v
HORIZONTAL 2μsec/cm
VERTICAL 1ma/cm (ACROSS 50 ohms)
50 ohm TERMINATION AT SCOPE
ACROSS 1000 ohm CURRENT
MEASURING RESISTOR

Figure 16 Oscillation in Ta_2O_5 Film with Single Pulse

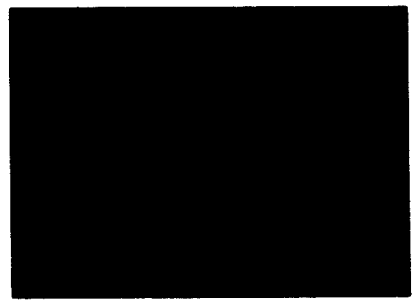

300 Å Al_2O_3 No breakdown
Single Pulse 10 μsec at 20 v
HORIZONTAL 2 μsec/cm
VERTICAL 5 ma/cm

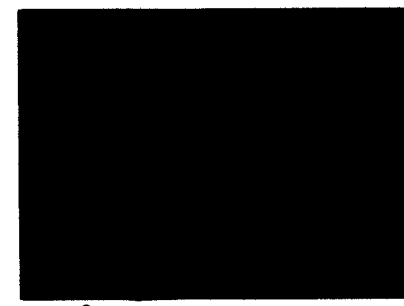

300 Å Al_2O_3 Single Pulse
10 μsec at 40 v
HORIZONTAL 2 μsec/cm
VERTICAL 10 ma/cm

300 Å Al_2O_3 10 μsec at 40 v
HORIZONTAL 5 μsec/cm
VERTICAL 20 ma/cm

300 Å Al_2O_3 10 μsec at 30 v
HORIZONTAL 2 μsec/cm
VERTICAL 10 ma/cm

Figure 17 Oscillation in Al_2O_3 Film with Single Pulse

ACKNOWLEDGEMENTS

It is a pleasure to acknowledge the encouragement of, and useful discussions with, Mr. J. P. Spratt and many other colleagues in this Laboratory. The author is also indebted to Messrs. T. Sikina, W. M. Kane, and W. C. Follmer for their assistance in preparing samples, and to J. Hetherington for his tireless assistance with the measurements.

APPENDIX A

CONDITIONS FOR SPUTTERING TANTALUM

SUBSTRATE

A. Microsheet Glass

B. Cleaning Procedure

1. detergent wash in ultrasonic cleaner
2. deionized water rinse
3. alcohol rinse

PROCEDURE

A. Pressure: 1×10^{-5} torr

B. Bleed in argon to 50 microns

C. Ta cathode cleaned in chamber by sputtering for 10 minutes; substrate surface masked during cleaning

D. Sputtering Rate: 300 Å/min. (2000 volts between plates and a current density of 150 ma./36 in^2 of electrodes surface area) Cathode Temperature: Approx. 400°C during sputtering.

APPENDIX B

CONDITIONS FOR EVAPORATION OF SiO

SOURCE

A. Drumheller Type (Allan Jones Co., Calif. holds 10 gm SiO)

B. Source to Substrate: 6-1/2 inches

PROCEDURE

A. Glow Discharge, to Clean System

1. Pump system to 1×10^{-5} torr
2. Bleed in argon to a few microns
3. Glow discharge: 5 min. at 1600 volts, 50 ma.
4. Pure Al rod cathode, substrate holder grounded

B. Deposition

1. Source Temperature: approx. 1300°C
2. Deposition Rate: approx. 10 Å/sec.
3. Pressure: $< 5 \times 10^{-6}$ torr (oil diffusion pumped system)

APPENDIX C

MEAN FREE PATH OF HOT ELECTRONS IN METAL FILMS*

This program was initiated at Philco at the beginning of 1962 to investigate the mean free path in metals of electrons having energies in the range 0.3 to 1.0 electron volts. The procedure is similar to that used by Spitzer[1] and involves forming a metal semiconductor diode and observing the photocurrent originating from electrons excited in the metal layer. The lowest energy for which a response can be observed is determined by the height of the barrier at the metal semiconductor interface; the highest energy is determined by the band gap of the semiconductor. Diodes studied under this program are silicon surface barrier diodes produced by the evaporation of various metals onto silicon surfaces.

The cleaving technique employed by Spitzer involved the use of several diode structures to observe photoresponse versus thickness. At the vacuum levels used in his experiment, the possibility existed of chemical contamination of all metals except gold. For this reason, it was felt that better results would be obtained if an ultra high vacuum system were used with the metal film thickness being built up in steps. This method allows photoresponse versus thickness to be obtained in a single diode structure and minimizes the effects of oxidation and gaseous contamination on the metals. Thus, an ultra high vacuum system was designed and built which was capable of 425°C bake-out and which allowed pressures of 5×10^{-10} torr. This pressure could be maintained for one month with this system closed off. Measurements of photoresponse have been obtained on gold-silicon diodes; the thickness of the gold film has been measured by depositing gold onto a quartz crystal calibrated against a multiple beam interferometer.

One such diode was measured for five different gold thicknesses, namely, 400, 550, 725, 880, and 1040 angstrons. Plots of photoresponse per incident photon as a function of photon energy were made for the last four thicknesses and are shown in Figure 1. From the data, a plot of response at a fixed energy as a function of thickness was obtained. This is shown in Figure 2 for 0.8, 0.9, and 1.0 electron volts. Based on optical measurements of these films, the assumption was made that the number of absorbed photons reaches a constant value by 550 angstrom units. Since the absorption range for gold in this energy range is about 130 angstrom units, if αt is greater than 1 and

---

* The work described in this paper represents Philco-supported work in the general area of interest to the subject contract.

1. Spitzer, et. al., Phys. Rev. Letters, Volume 8, (1962) pp. 57-58.

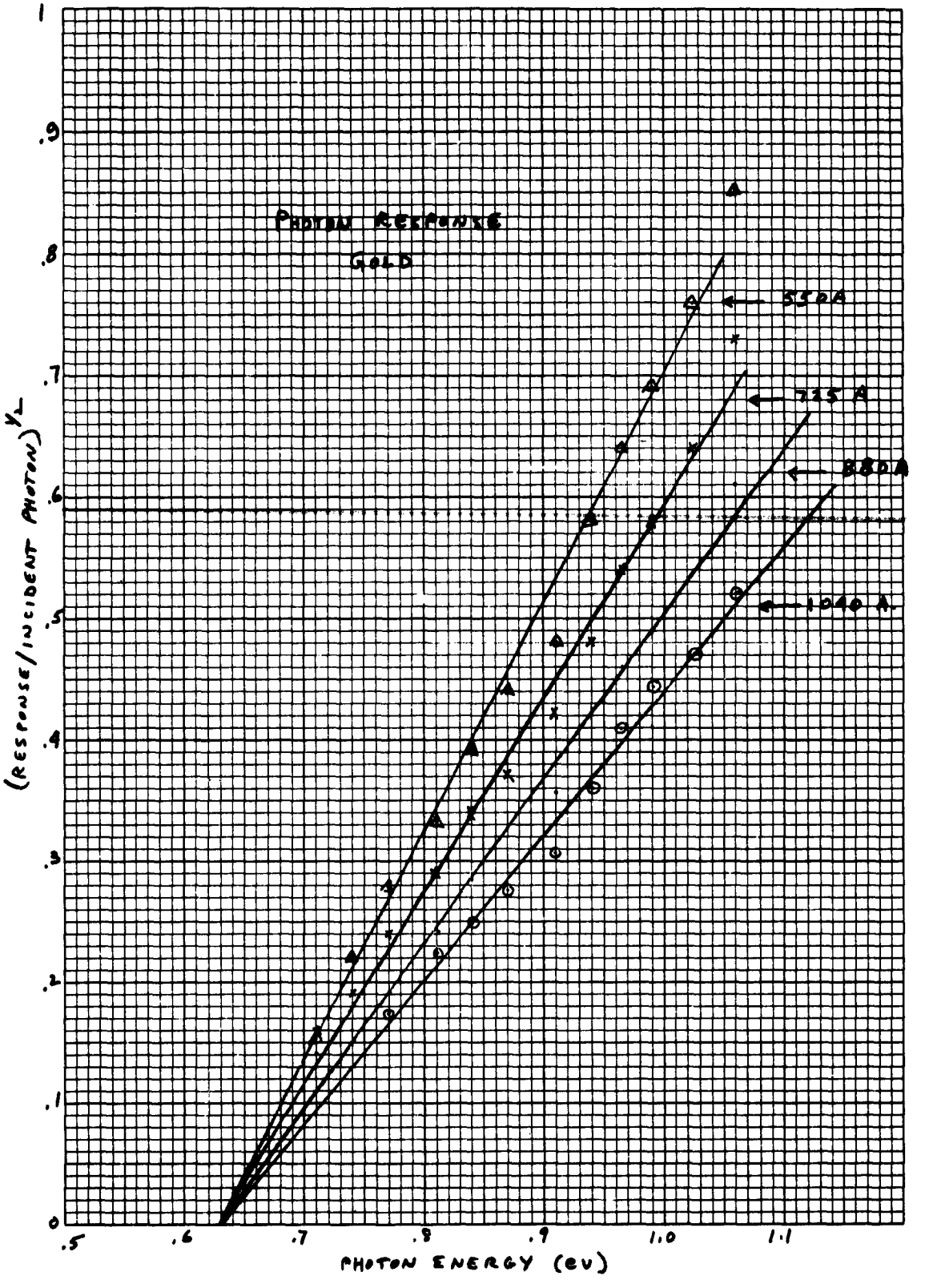
PHOTON RESPONSE
GOLD
550 A
725 A
880 A
1040 A
(RESPONSE/INCIDENT PHOTON) Y_L
PHOTON ENERGY (eV)
0
.1
.2
.3
.4
.5
.6
.7
.8
.9
1
.5
.6
.7
.8
.9
1.0
1.1

Figure 1

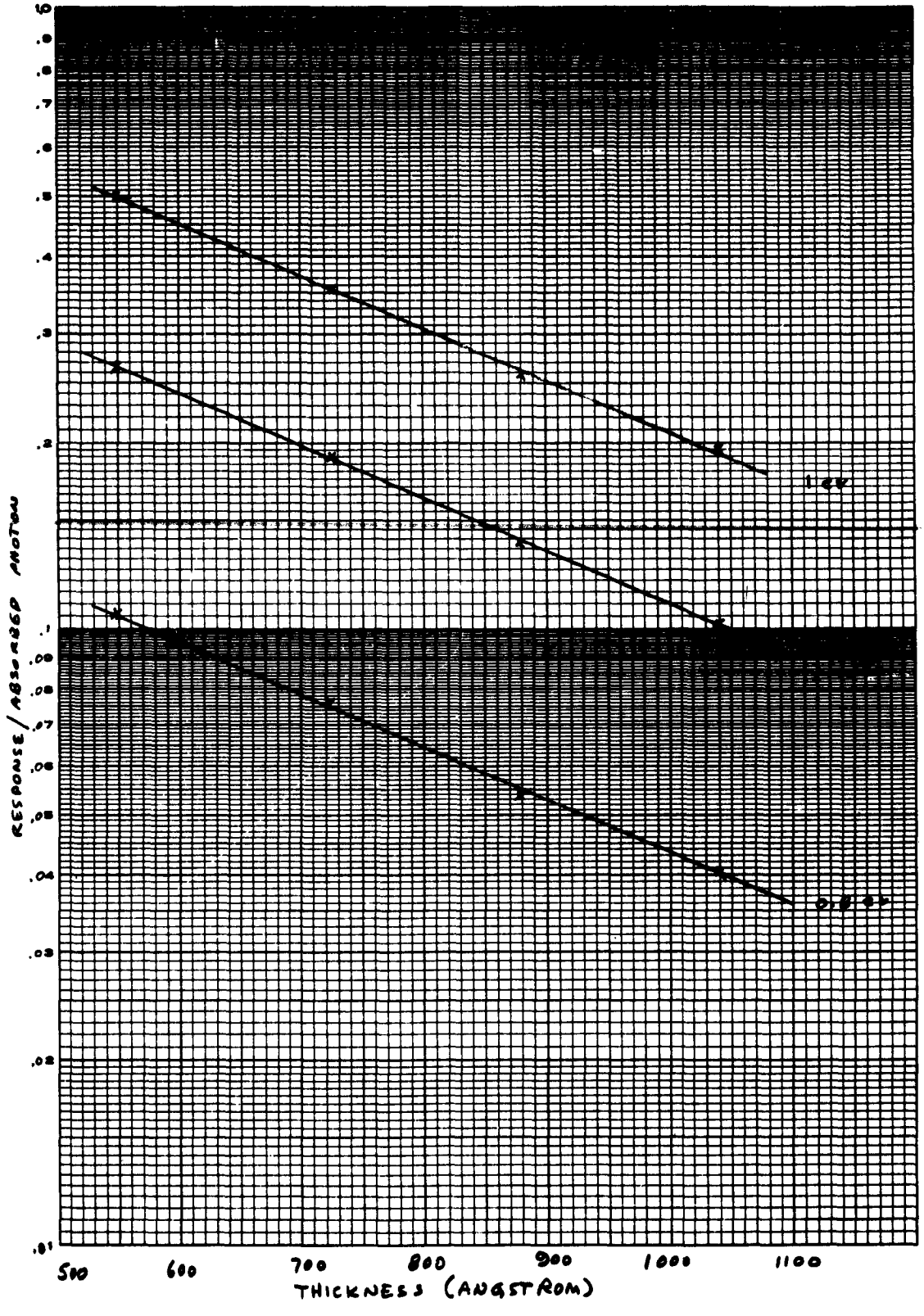
RESPONSE/ABSORBED PHOTON
.5
.6
.7
.8
.9
.4
.3
.2
.1
.09
.08
.07
.06
.05
.04
.03
.02
.01
1 eV
0.8 eV
500
600
700
800
900
1000
1100
THICKNESS (ANGSTROM)

Figure 2

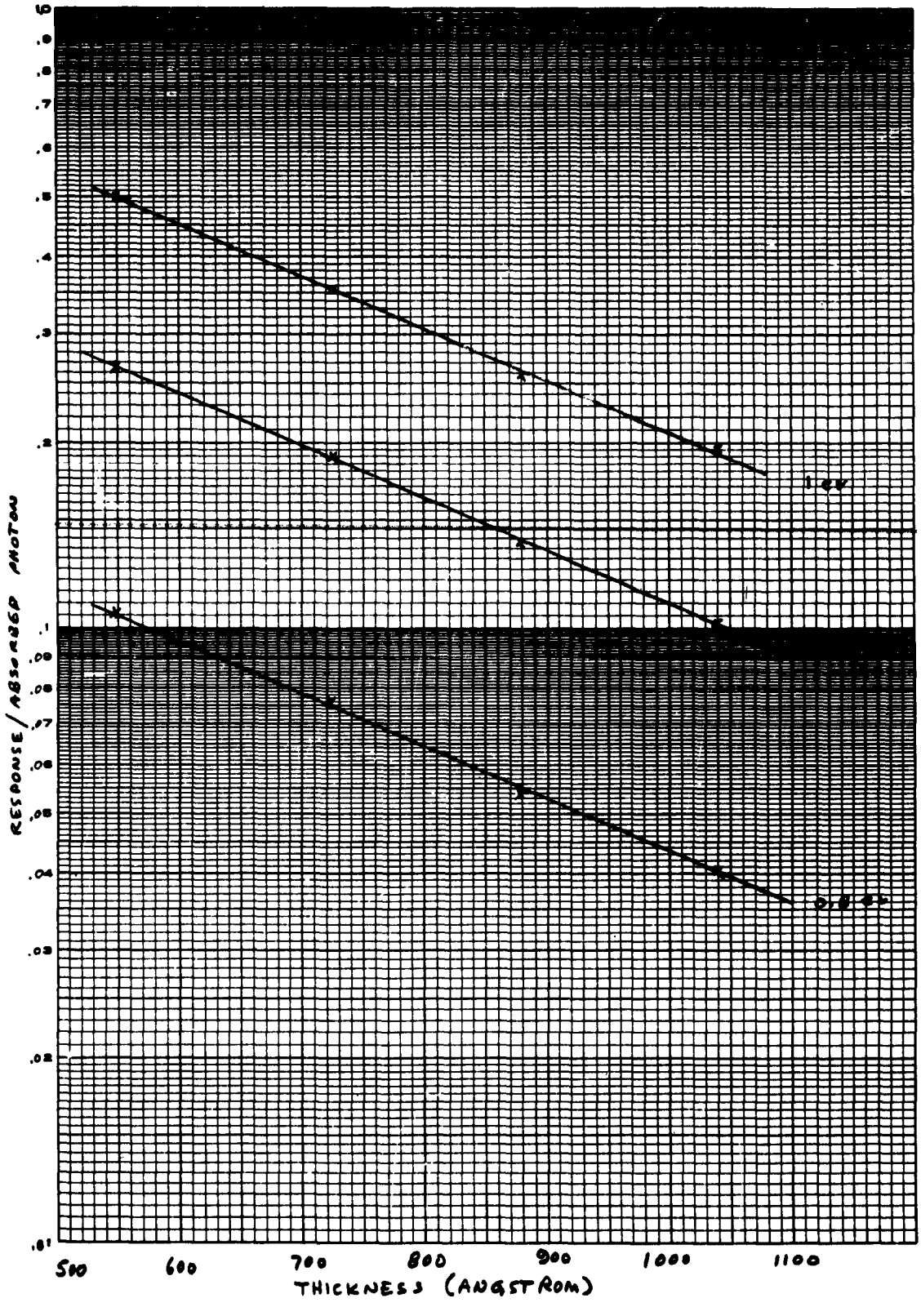
RESPONSE/ABSORBED PHOTON
.6
.5
.4
.3
.2
.1
.09
.08
.07
.06
.05
.04
.03
.02
.01
500
600
700
800
900
1000
1100
THICKNESS (ANGSTROM)
1 eV

Figure 2

if L is very much greater than $1/\alpha$ (t is equal to the film thickness and L is equal to the mean free path), then the response for per absorbed photon, R, is proportional to $e^{-t/L}$, and the slope of the lines in Figure 2 will give the mean free path. A value of L = 510 angstroms was obtained for gold. Since this value is substantially below that obtained by Spitzer for gold, these measurements will be repeated during the next quarter and attempts will be made to obtain similar measurements on other metals of interest such as aluminum.

APPENDIX D
BIOGRAPHIES OF KEY PERSONNEL*

William C. Follmer, Research Specialist

Mr. Follmer received a B.S. degree in electrical engineering from Pennsylvania State University in 1956.

Since joining Philco in June 1956, he has been engaged in semiconductor research, specializing in evaluating new devices and the development of new methods of device measurement and fabrication.

Mr. Follmer has assisted in the development of techniques for making noise figure measurements on transistors and in designing equipment for measuring microalloy graded-base transistors with millimicrosecond switching times. He designed and developed transistorized electronic systems for infrared imaging and detection. He has also worked on tunnel diode circuitry, los-noise preamplifiers, and the noise theory of semiconductor devices.

Recently, Mr. Follmer's work included design and testing of microminiature digital circuits, and work on a theoretical and experimental study of tunnel diode mixers, characterization of the UHF coaxial transistor, and evaluation and characterization of the metal interface amplifier.

Mr. Follmer is the author of the following paper:

"Low Frequency Noise in Background Diodes," Proceedings of the IRE, December 1961.

He is also coauthor of a presentation entitled "A Tunnel Emission Triode" at the Device Conference in Washington, D. C. (coauthors: R. F. Schwarz, et. al

Mr. Follmer is a Member of the IEEE, Eta Kappa Nu, and Sigma Tau.

* NOTE: Biographies of other key personnel have been submitted as an Addendum to the First Quarterly Report under this contract